5-2021

Sonic Boom Loudness Reduction Through Localized Supersonic Aircraft Equivalent-Area Changes

Troy A. Abraham
Utah State University

SONIC BOOM LOUDNESS REDUCTION THROUGH LOCALIZED SUPERSONIC AIRCRAFT EQUIVALENT-AREA CHANGES

by

Troy A. Abraham

A thesis submitted in partial fulfillment
of the requirements for the degree

of

MASTER OF SCIENCE

in

Mechanical Engineering

Approved:

Douglas F. Hunsaker, Ph.D. Major Professor	Stephen A. Whitmore, Ph.D. Committee Member
Matthew W. Harris, Ph.D. Committee Member	D. Richard Cutler, Ph.D. Interim Vice Provost of Graduate Studies

UTAH STATE UNIVERSITY
Logan, Utah

2021

ABSTRACT

Sonic Boom Loudness Reduction Through Localized
Supersonic Aircraft Equivalent-Area Changes

by

Troy A. Abraham, Master of Science
Utah State University, 2021

Major Professor: Douglas F. Hunsaker, Ph.D.
Department: Mechanical and Aerospace Engineering

This work explores the design space created from modeling the effect of localized geometric changes on a supersonic aircraft's near-field pressure signature. These geometric changes are used to alter the aircraft's near-field pressure signature in a way that reduces its sonic boom loudness at the ground. The aircraft used in this work is the NASA 25D concept and its near-field pressure signature is modeled using two separate approaches. The first approach uses the PANAIR panel code to obtain a near-field pressure signature for an axisymmetric representation of the 25D. This near-field signature is propagated to the ground using the NASA sBOOM propagation code and the perceived level in decibels is calculated using an in-house loudness code called PyLdB. The second approach uses the equivalent-area distribution of the 25D which is passed directly to sBOOM and the perceived level is also found using PyLdB. To model the geometric changes, the axisymmetric geometry and the equivalent-area distributions are first independently modified with a parameterized Gaussian deformation. An extension to the equivalent-area approach using larger splined deformations is also implemented. These methods are fast enough to quickly explore the design space and find the change in loudness for different deformation parameters. This design space exploration is used to study loudness changes for both on-design conditions

and the effects of deviations from on-design angle of attack, Mach number, and azimuth angle. Both a genetic algorithm and a gradient search method are used in these off-design atmospheric and flight condition studies. These results can be used to inform higher fidelity CFD studies, including an inverse geometry design problem, and structural adaptation design on the aircraft. The combination of speed and flexibility of the methods used in this work make them desirable over using higher fidelity tools independently to perform these studies.

(87 pages)

PUBLIC ABSTRACT

Sonic Boom Loudness Reduction Through Localized
Supersonic Aircraft Equivalent-Area Changes
Troy A. Abraham

The NASA University Leadership Initiative (ULI) titled "Adaptive Aerostructures for Revolutionary Civil Supersonic Transportation" looks to study the feasibility of distributed structural adaptivity on a supersonic aircraft for maintaining acceptable en-route sonic boom loudness during overland flight. The ULI includes a team of industry and university partners that are working together to develop and implement the systems necessary to accomplish this goal.

The Utah State University Aerolab is a member of this ULI team and has been tasked with developing and using low-fidelity supersonic aerodynamic and sonic boom predictions tools to rapidly study the effects of localized geometry changes on a supersonic aircraft's sonic boom loudness. The current work utilizes the equivalent-area distribution of a supersonic aircraft to study the effects of these localized geometry changes.

The speed of these low-fidelity tools gives them an advantage over the higher fidelity computational methods such as CFD. The low-fidelity tools used in the current work allow for the study of thousands of geometric changes over a variety of flight conditions in a relatively small amount of time. The results of these studies provide areas of sensitivity that can be used in the higher fidelity CFD work as well as initial actuator and structural design.

Dedicated to my mother and father...

ACKNOWLEDGMENTS

I owe a debt of gratitude to my advisor Dr. Hunsaker for providing me the opportunity to work and learn from him over the course of the last few years. Low-fidelity supersonics has proven to be a complicated, yet fascinating, area of research that continues to provide new avenues for tool development and study. I also owe thanks to my partner and the many friends, colleagues, and close family members that have supported me and lent me their time and insight throughout my education.

I would also like to thank Jonathan Weaver-Rosen and Pedro Leal from Texas A&M University for their contributions to this work.

This work is supported by the NASA *University Leadership Initiative* (ULI) program under federal award number NNX17AJ96A, titled "Adaptive Aerostructures for Revolutionary Civil Supersonic Transportation."

Troy A. Abraham

CONTENTS

LIST OF TABLES

LIST OF FIGURES

ACRONYMS

AoA	Angle of attack
AXIE	Axisymmetric geometry
CFD	Computational fluid dynamics
OML	Outer mold line
PLdB	Perceived level of loudness in decibels
ULI	University Leadership Initiative
A_{Eq}	Traditional total equivalent area
$A_{E,r}$	Reversed total equivalent area
A_L	Equivalent-area contribution from lift
A_V	Equivalent-area contribution from volume
L_x	Longitudinal lift distribution
M	Mach number
M_∞	Freestream Mach number
Δp	Overpressue, $= p - p_\infty$
p_∞	Ambient pressure
R	Radial distance
u_∞	Freestream velocity
β	Prandtl-Glauert factor, $= \sqrt{M^2 - 1}$
γ	Ratio of specific heats, $= 1.4$
μ	Mach angle, $= \sin^{-1} \frac{1}{M}$
ρ	Freestream air density
ϕ	Azimuth angle

CHAPTER 1

INTRODUCTION

1.1 The Sonic Boom Problem and Motivation for the Current Work

The sonic booms produced by supersonic aircraft have been a subject of study since the early 1960s. Efforts to bring supersonic aircraft into commercial use have been limited due to the annoyance of the sonic boom loudness to human populations as well as the sonic boom's potential for causing structural damage [1]. Because of these side effects, supersonic flight over the United States is currently restricted and commercial flights in the past have been limited to over-water operation routes [2]. In an effort to overcome the current restrictions to supersonic flight, a number of studies have been performed that explore modifying an aircraft's geometry to change its pressure signature and reduce its sonic boom loudness to a level permissible for overland flight [1, 3]. The current work is a continuation of these geometry changing efforts and utilizes many of the same fundamental supersonic concepts.

The phenomenon of the sonic boom is a result of the aerodynamics of an aircraft traveling faster than the speed of sound. More specifically, it is the generation of shock waves and their influence on the local flow field that creates a sonic boom. These shock waves are regions where nearly instantaneous changes in flow properties occur over very small distances [4]. The change in pressure across a shock wave is the most important property to consider when studying an aircraft's sonic boom. Specific features of these shock waves and their interactions are captured in what is referred to as a pressure signature. A pressure signature is typically represented as a plot of the change in pressure relative to ambient pressure, also known as overpressure, with respect to either time or distance. Shock waves are seen as sudden jumps in overpressure. A typical pressure signature sampled near a supersonic aircraft will have multiple regions of shock and expansion features where the

overpressure either jumps rapidly or slowly returns towards, and sometimes below, ambient pressure. As these shock waves propagate away from the aircraft they begin to coalesce into larger shock waves. The coalescence of these shock waves, generally referred to as pressure signature aging, often results in pressure signatures that take on the familiar "N-wave" shape at the ground. It is the large changes in overpressure, typical of the front and rear portions of an N-wave signature, that are perceived as sonic booms.

There are three regions where pressure signatures are generally classified, each defined by their distance from a supersonic aircraft. The pressure signatures nearest the aircraft, within a few body lengths, are called near-field signatures. Signatures more than a few body lengths away and signatures at the ground are known as mid-field signatures and ground signatures respectively. Figure 1.1 shows a notional example of how the features of these signatures might develop as they propagate to the ground. Previous efforts, such as the Shaped Sonic Boom Demonstrator [3], have shown that it is possible for an aircraft to generate a near-field signature that does not fully develop into the typical N-wave ground signature. Significant work has been done in an effort to establish methods for designing supersonic aircraft configurations that produce ground signatures with shock features that are desirable for minimizing the annoyance of a sonic boom [5–8].

These modern supersonic aircraft design techniques have lead to configurations that achieve ground level perceived loudness values that are much smaller than previous supersonic aircraft. For example, the NASA 25D concept aircraft was shown to have a ground level perceived loudness of about 78 dB [9]. This is much lower than the 105 dB sonic boom produced by the Concorde [10]. These advances in supersonic aircraft design have ushered in a new era of potential supersonic commercial flight with permissible ground level perceived loudness values.

An additional challenge that will influence how commercial supersonic flight is regulated is the effect of off-design flight conditions on the perceived loudness. It has been shown that changes to flight conditions such as Mach number, angle of attack, and local atmospheric profiles can have large negative effects on the perceived loudness at the ground [11]. Because

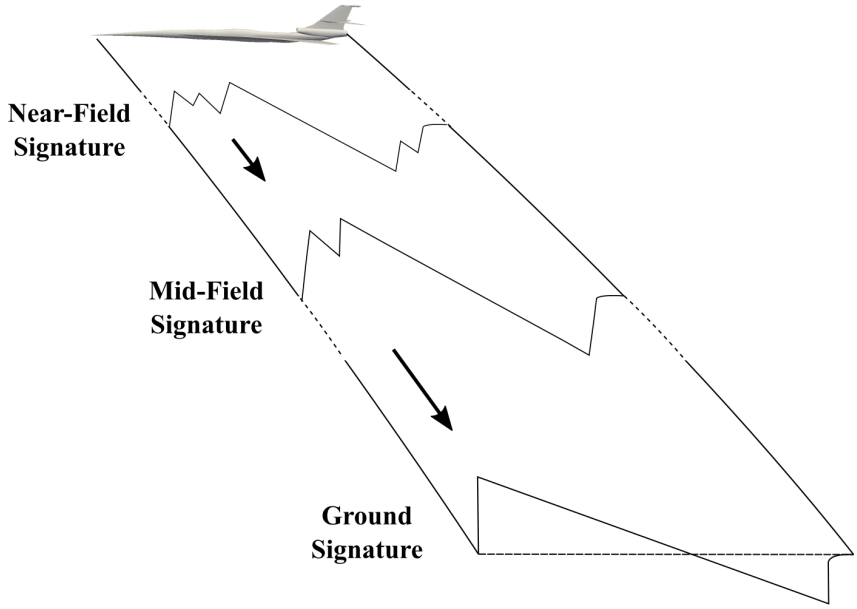

Fig. 1.1: Supersonic aircraft pressure signature regions and propagation.

of these off-design effects, there is a desire for methods capable of actively responding to these flight conditions to mitigate the degradation of an aircraft's sonic boom loudness during flight. One such method might employ active localized aircraft geometry changes to influence the local supersonic flow field. The methods for identifying the required geometry changes to achieve these sonic boom loudness improvements are the subject of the current work.

1.2 University Leadership Initiative - Adaptive Aerostructures for Revolutionary Civil Supersonic Transportation

The current work is part of a NASA University Leadership Initiative titled "Adaptive Aerostructures for Revolutionary Civil Supersonic Transportation", hereafter referred to as the ULI. The ULI is studying the feasibility of using localized aircraft outer mold line (OML) structural adaptivity to reduce an aircraft's sonic boom loudness at the off-design flight conditions mentioned previously. Identifying and implementing the OML changes required to return an aircraft's perceived loudness to permissible levels for overland flight

would expand the range of its realizable operating conditions. The current work is done in support of the overall ULI objective.

1.2.1 University Leadership Initiative - Previous USU Work

The work of the Utah State University Aerolab within the ULI has focused on low-fidelity aerodynamic and sonic boom prediction tools. Previous work by Giblette utilized the PANAIR panel code within a sonic boom prediction framework [12]. PANAIR was used to generate the surface pressure solution for a supersonic body as well as sampling of the off-body pressure signature [13]. A major challenge that Giblette addressed was developing a method for automated PANAIR mesh generation utilizing preexisting unstructured CFD meshes. Generating the structured PANAIR mesh from an existing CFD mesh ensured the geometric errors between solutions were minimal [14]. The work of Giblette was successful to some extent but ran into issues with limitations on the number of panels that could be used within PANAIR as well as violations of a number of the linear supersonic assumptions when trying to generate the surface pressure distributions on more complex geometries. Breaking these assumptions resulted in numerical errors in the surface pressure solution and large, non-physical, shock characteristics in the near-field. Bolander attempted to remedy this issue by splicing the usable forward portion of the PANAIR near-field signature with a correct aft signature [15]. He found limited success in applying this technique once modifications to the aircraft's OML were applied.

In addition to PANAIR, the sonic boom prediction framework developed by Giblette includes an atmospheric propagation code called sBOOM. sBOOM is a code developed by NASA that numerically solves the Augmented Burgers Equations and includes the effects of thermosviscous absorption and molecular relaxation [16]. sBOOM can take a pressure signature, equivalent-area distribution, and F-function, each effectively a different representation of a supersonic aircraft's pressure signature, as input. sBOOM does not assume a zero shock thickness, like previous atmospheric propagation models, and can take atmospheric inputs such as humidity, temperature, and wind profiles. These features make sBOOM ideal for application within the current work and the ULI as a whole.

In the context of Figure 1.1, PANAIR is used to generate the near-field pressure signatures and sBOOM is used to propagate them through the atmosphere to obtain the ground signatures. The mid-field signatures can be found using sBOOM to propagate to intermediate altitudes if desired. The final step in the sonic boom prediction framework is estimating the loudness of the ground signature. A code called PyLdB was developed by Bolander as an open source pressure signature loudness tool [17]. This code is based on Stevens' Mark VII method for calculating the perceived level in decibels (PLdB) and has been benchmarked against other widely used sonic boom loudness tools [18] [1].

Figure 1.2 demonstrates the sonic boom prediction framework outlined here. This framework forms the foundation of the studies outlined in the current work. Additional methods for representing an supersonic aircraft's near-field pressure signature will be discussed in the literature review chapter that follows.

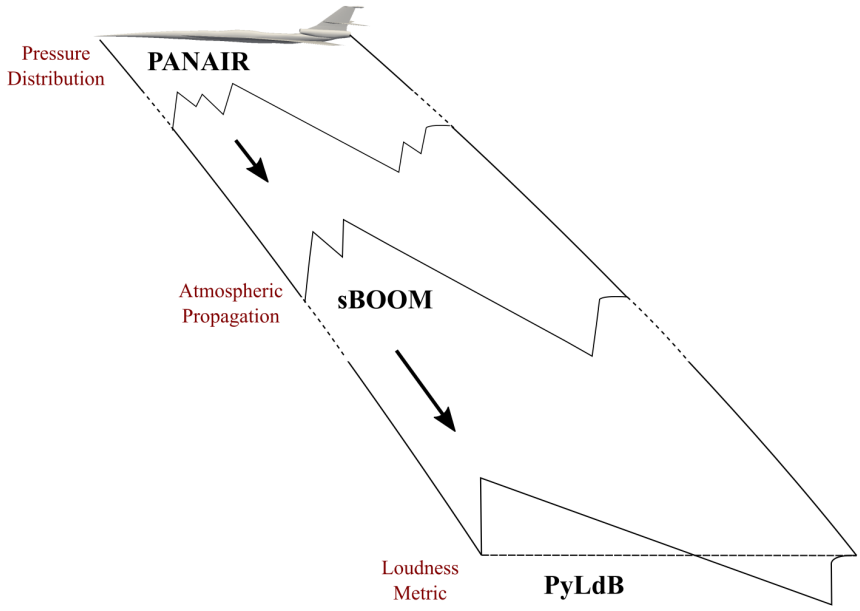

Fig. 1.2: Sonic boom prediction framework.

[1] https://github.com/usuaero/PyLdB

1.2.2 University Leadership Initiative - Current USU Work

The studies specific to the current work utilize low-fidelity methods to explore the design space created from the localized geometric changes to an aircraft's OML. Two general low-fidelity methods are used in this work and are described in detail in the computational methods chapter that follows. The NASA 25D concept aircraft and its axisymmetric representation, as provided by the 2017 2nd AIAA Sonic Boom Prediction Workshop, are the aircraft geometries that are studied in this work [9].

The design space exploration begins with identifying simple OML changes that reduce loudness in a standard atmospheric profile. These results are used to constrain a genetic algorithm implemented to find optimum changes to the OML for a number of different atmospheric conditions. This optimization is initially performed using a single geometry change and then is expanded to include a second. The design space exploration is then advanced to include the effects of off-design flight conditions such as Mach number, angle of attack, azimuth angle, and atmospheric profiles. These off-design studies are initially done using the single geometry change but a second method is utilized that is capable of larger continuous changes. These larger changes are found to be necessary to achieve a higher level of sonic boom loudness reduction. Additionally, a brief comparison of the effects of unpowered and powered models of the 25D is made. The results of this work are used to identify the locations and magnitudes of geometric changes that can be used in higher fidelity inverse design studies and by a design team developing an adaptive structure capable of morphing in flight.

The low-fidelity methods outlined in the current work offer significant time savings over higher fidelity methods, such as CFD or panel methods, when exploring a design space such as the one described here. When using CFD, studying the effects of small changes to an aircraft's geometry often requires running entire solutions for each iteration. These CFD solutions become cumbersome and intractable when the design space includes hundreds or thousands of possible changes. The low-fidelity methods used here offer a first-order approach for identifying the locations and magnitudes that are most sensitive to geometric

changes. While the low-fidelity solutions do not contain exact information about the changes to a full aircraft, they can significantly reduce computation time by narrowing down the types of solutions that should be explored using the higher fidelity methods.

The methods outlined in the current work are especially well suited for the goal of the ULI in identifying locations to implement distributed discrete OML structure adaptation. These methods could also prove useful in preliminary supersonic aircraft design where the baseline OML needs to be designed to meet some sonic boom loudness constraint. The current tools could be used to identify problem areas of an OML and estimate the required adjustments to the geometry. The simplicity of these methods provides ample opportunity for additional customization and application to different supersonic aircraft under different flight conditions.

CHAPTER 2

LITERATURE REVIEW

A wide range of theories and tools have been developed to study the physics of the creation and propagation of sonic booms. These tools vary in fidelity and application and each have their own limitations and advantages. The current chapter looks to summarize a number of these tools and theories and present them in the context of a modern sonic boom prediction framework.

Most modern supersonic tools and methods still use concepts rooted in the classical linear supersonic theory. Linear supersonic theory involves estimating the flow around a super sonic body using linear approximations within the equations describing the full three dimensional flow. The result of these approximations are equations that capture the most important aspects of the flow around the supersonic body, but at the cost of some accuracy. This approach is used in estimating the wave drag of a supersonic body and has produced well known solutions such as the supersonic area rule and the Sears-Haack body [19–21]. In its application to sonic booms and off body pressure predictions, linear theory predicts disturbances that move along parallel characteristic lines. These parallel characteristic lines have proved to be incorrect and modifications to the original linear theory were made by Whitham [22]. Whitham developed a way to model non-linear effects that produced curved characteristics. The modificaitons to linear theory by Whitham became known as modified linear theory which provides the foundation for many of the concepts that follow.

2.1 Classical Sonic Boom Theory - Equivalent Area

The first and most relevant sonic boom theory that is applied in the current work is the concept of the supersonic equivalent area. The supersonic equivalent area is describe in detail in the literature by Plotkin, Carlson and Maglieri, and Seebass [23–25] with the

description by Carlson and Maglieri being especially good for gaining a conceptual understanding of the subject. The information contained within those documents forms the basis for the summary that is provided here.

The premise of the supersonic equivalent area is that the pressure disturbances caused by an arbitrary three dimensional body traveling at supersonic speeds can be viewed as originating from a body of revolution with the same distribution of area as the original three dimensional body. There are two major contributions to the equivalent area that must be represented by this body of revolution. The first is the geometric area distribution of the original supersonic body. The second is an area distribution that is a function of the longitudinal distribution of lift. Equation (2.1) is the relationship for the area from lift contribution as an integration along the body.

$$A_L(x,\phi) = \frac{\beta}{\rho u_\infty^2} \int_0^x L(t,\phi)\, dt \tag{2.1}$$

Here t is a dummy variable of integration. The total equivalent area is a superposition of the area from volume and the area from lift, as shown in Eq.(2.2)

$$A_{Eq}(x,\phi) = A_V(x,\phi) + A_L(x,\phi) \tag{2.2}$$

Here ϕ is an azimuth angle around the supersonic body, indicating there is a different equivalent-area distribution at each azimuth angle. The distribution of ϕ is demonstrated in Fig. 2.1.

For Mach numbers greater than one, the distribution of lift and area must be found using cuts taken by the fore Mach cone defined in an observers frame of reference. The fore Mach cone represents the domain of influence a particular supersonic body will have on a observer. The shape of this fore Mach cone is a result of the manner in which the pressure disturbances, traveling at the speed of sound, propagate relative to a body moving faster than the speed of sound. It is at the instance that a supersonic body crosses the surface of the fore Mach cone that an observer, some distance below the body, begins to

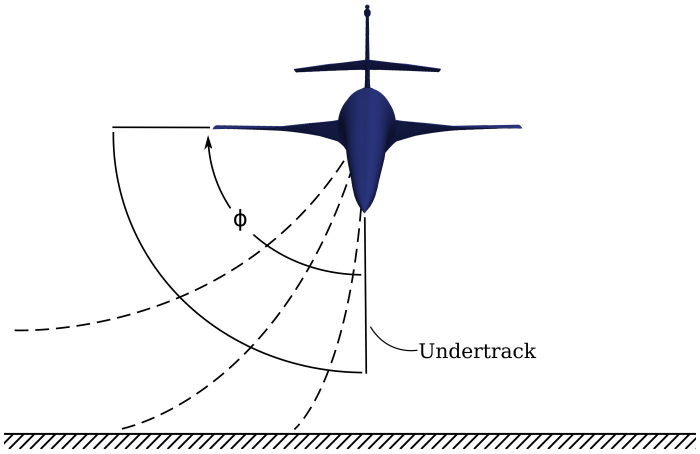

Fig. 2.1: Azimuth angle relative to a supersonic body.

feel its influence. The distribution of the body's area and lift are what ultimately create the disturbances felt by the observer. At distances far enough away from the body, these fore Mach cone cuts can be approximated using tangent planes inclined at the freestream Mach angle. The fore Mach cone and the Mach angle inclined planes are demonstrated in Fig. 2.2 and Fig. 2.3 respectively.

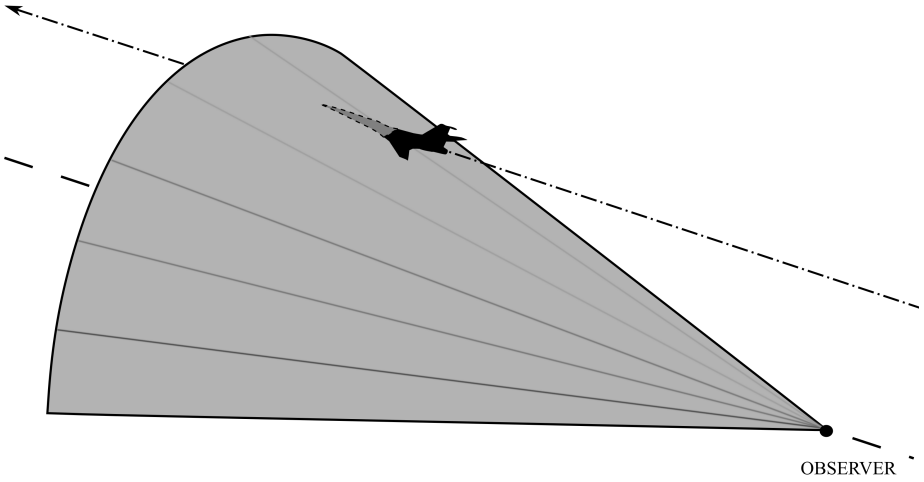

Fig. 2.2: Fore Mach cone.

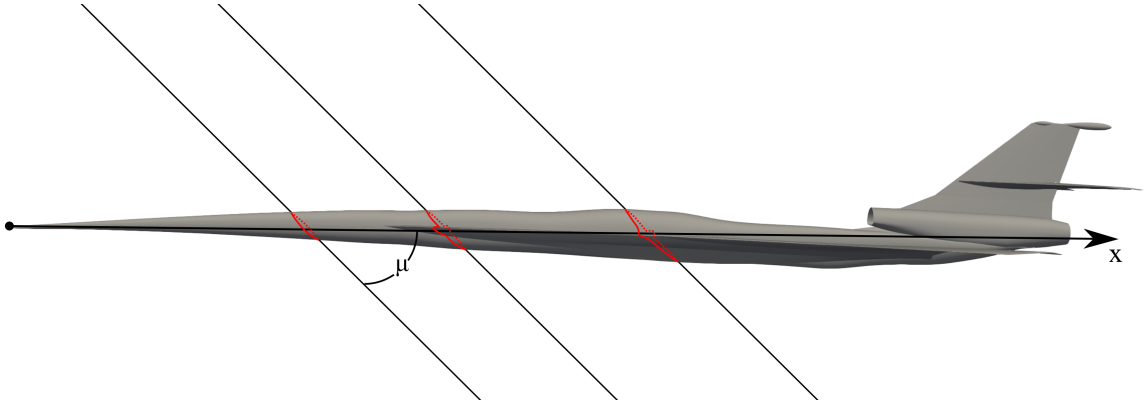

Fig. 2.3: Tangent Mach plane slices.

For the geometric area, the Mach plane cut area is projected onto a constant x plane, normal to the freestream. The lift distribution used in the integration of Eq.(2.1) is the net force normal to the freestream acting on the perimeter of a particular Mach plane cut [25]. Again, the superposition of these two area contributions results in the total equivalent area. Under this traditional formulation of equivalent area, the peak value of the equivalent area during steady level flight is defined by the total weight of the aircraft. The total equivalent-area distribution appears in the relationship for the Whitham F-function shown in Eq.(2.3).

$$F(x,\phi) = \frac{1}{2\pi}\int_0^x \frac{A''_{Eq}(t,\phi)}{\sqrt{x-t}}\,dt \tag{2.3}$$

The Whitham F-function is an intermediate value that maps the distribution of area back to its influence on pressure disturbances. Many of the original sonic boom minimization efforts worked with the F-function directly [26, 27]. Equation (2.4) shows the relationship between the Whitham F-function and overpressure.

$$\Delta p(x,\phi,R) = p_\infty \frac{\gamma M^2 F(x,\phi)}{\sqrt{2\beta R}} \tag{2.4}$$

The relationships between the equivalent-area distribution and the off-body pressure signature allow for estimating how changes to an aircraft's equivalent area, through either volume or lift contributions, will affect the aircraft's off-body pressure signature and ultimately its sonic boom loudness. This approach has been used in a number of studies where

changes in the volume of an aircraft were used to approach some low boom equivalent-area goal [5, 6, 28]. The general approach of making changes to an equivalent-area distribution in place of modifying a full 3D geometry configuration is the basis of the current work.

2.2 Reversed Equivalent Area

The traditional methods of generating an aircraft's equivalent-area distribution generally involve Mach plane slicing, as was outlined in the previous section. This process begins with solving or estimating the surface pressure distribution around a supersonic body and then performing the necessary slicing and integration to solve Eq.(2.1) and Eq.(2.2). Using the surface pressure in this manner inherently ignores additional 3D flow effects that occur within the immediate vicinity of a supersonic aircraft [7]. With the advent of modern CFD tools, pressure distributions can be sampled around a supersonic aircraft at some desired radial distance. This allows the 3D flow effects to further develop before the pressure is sampled. If the sampling occurs far enough away from the aircraft it can be assumed that the pressure distribution has fully developed and is now linear with propagation distance relative to the aircraft.

The ability to sample a near-field pressure signature from a CFD solution has lead to an alternative approach for generating an equivalent-area distribution. Li and Rallabhandi outline this approach and provide the necessary equation for applying this to a near-field pressure signature [7]. The concept uses the Whitham F-function, Eq.(2.3), and its relationship to the overpressure, Eq.(2.4), to solve for the equivalent-area distribution. The result is the equation presented by Li and Rallabhandi and is shown here in Eq.(2.5)

$$A_{E,r}(x) = 4\frac{\left(2R\sqrt{M_\infty^2 - 1}\right)^{\frac{1}{2}}}{\gamma M_\infty^2} \int_0^x \frac{\Delta p}{p_\infty}(t - x_0)\sqrt{x - t}\, dt, \tag{2.5}$$

Here R is the radial distance away from the aircraft that the pressure distribution was sampled. This approach has been used in a number of previous equivalent-area matching studies [6, 7, 28] and provides more accurate estimates of an aircraft's sonic boom loudness. Relative to the current work, the process of generating an equivalent area from a CFD

near-field solution provides a stronger link between the low-fidelity sonic boom prediction framework and the higher fidelity CFD solutions.

A challenge of this process arises when considering how a change to equivalent area translates to the full 3D geometry. Because the reversed equivalent area is no longer the superposition of volume and lift effects alone, it becomes much more difficult to inversely model how an equivalent-area change relates to one or both of the traditional equivalent-area contributions. The scope of this problem will not be covered in the current work but one known method is commonly referred to as an inverse design scheme. The premise of the inverse design is to utilize a free form deformation tool to modify a CFD mesh until the resulting pressure signature produces an equivalent area that matches the modified equivalent-area distribution target [7].

Within the scope of the ULI, the results of the current work are provided to the CFD teams to perform an inverse design, as it has been described here. Details of this process are omitted here but the work by Weaver-Rosen et al outlines one approach to implementing this process in a larger sonic boom minimization framework [29].

2.3 Signature Propagation and Atmospheric Effects

Methods for propagating a pressure signature to the ground have evolved extensively over the history of sonic boom research. Early calculations were based in linear and modified linear theory and could be done without the use of a computer [22]. As more consideration towards the effects of real atmospheres was made, it became necessary to model the propagation using computer algorithms. Many of these computer algorithms were based in linear and modified linear theory and were incapable of predicting shock rise times and shock merging. Because sonic boom loudness metrics are highly dependent on the frequency content of a signature [30], the empirical methods that could be used to modify the linear results and estimate shock rise times were often inadequate [16, 18].

To overcome the issues encountered within linear theory, researchers such as Rallabhandi began using a modified form of the Burgers equation. The code written by Rallabhandi, known as sBOOM, implements various improvements that account for absorption,

molecular relaxation, and atmospheric stratification [16]. sBOOM also includes the ability to use an F-function, equivalent area, or pressure signature as input. Additional features of sBOOM include its ability to handle inputs for non-standard atmospheres including temperature and humidity distributions and stratified wind profiles. The ability to estimate finite shock rise times and an extensive array of input options has made sBOOM a widely used atmospheric propagation code. It is the propagation method that is used in the current work.

2.4 Low Boom Aircraft Design - NASA 25D

The results presented in the current work are focused on a single aircraft configuration to demonstrate the methods and tools used. This aircraft is the NASA 25D concept which was the subject of study of the 2017 2nd AIAA Sonic Boom Prediction Workshop (SBPW) [9]. The 25D configuration was originally designed to demonstrate a number of the tools, mentioned previously, for generating an outer mold line capable of meeting some low boom PLdB goal in a standard atmospheric profile. Trim conditions and full carpet boom loudness were also influential on the original design of the 25D [31, 32]. It is worth noting that the SBPW used 4 distinct representations of the 25D and its near-field signature. The first was an axisymmetric geometry, the second was a wing-body configuration, and the final two were the full 25D with and without a powered engine nacelle. The majority of the results shared in the current work focus on the axisymmetric geometry and the 25D with a flow-thru engine nacelle. Because of the large amount of existing studies, data, and computational meshes available, the 25D provided a good starting point to test the off-design localized OML changes proposed by the ULI and the current work. The on-design cruise flight conditions of the 25D are a Mach number of 1.6 and an angle of attack of 3.375°.

CHAPTER 3

COMPUTATIONAL METHODS AND TOOLS

There are three sets of tools used in this work to explore the design space of geometric changes to a supersonic aircraft with the goal of reducing its sonic boom loudness. The first method produces a near-field pressure signature using the PANAIR panel code and the axisymmetric geometry representation of the aircraft's equivalent area. Previous work has demonstrated that PANAIR can be used to produce good near-field results for the 25D's axisymmetric geometry [12]. The near-field signature found using PANAIR is passed to the NASA sBOOM Sonic Boom Propagation code to produce a ground signature. The ground signature produced by sBOOM is analyzed using an in-house code called PyLdB to estimate the sonic boom loudness at the ground. This code is based on Stevens' Mark VII method for calculating the perceived level in decibels (PLdB) [1]. The studies done using this method apply small changes to the axisymmetric geometry before generating the near-field pressure signature.

In the second method, the aircraft's equivalent-area distribution is passed directly to sBOOM. This removes the need of PANAIR for producing the near-field pressure signature. sBOOM propagates the resulting pressure signature to the ground and the loudness is calculated using PyLdB. In this method, the studies are done using small discrete changes to the equivalent area before each resulting pressure signature is propagated to the ground. In the third method, larger continuous changes are made to the equivalent area before the resulting pressure signature is propagated to the ground. Each of these methods is described in detail in the sections that follow.

[1] https://github.com/usuaero/PyLdB

3.1 Axisymmetric Geometry and PANAIR Panel Code

The axisymmetric geometry method, hereafter referred to as AXIE, is used to explore the design space of small geometric changes to the OML of the 25D and their effect on PLdB at the ground. The geometry used was provided by the 2017 2nd AIAA Sonic Boom Workshop and the PANAIR panel solution using this geometry was studied extensively in previous work by Giblette [12]. The small geometry changes are achieved by modifying the radius of the AXIE PANAIR mesh with a parameterized Gaussian function to add a single deformation at some axial location. The Gaussian deformation is specified with a length equivalent to one standard deviation, a height or amplitude, and the axial location on the geometry, as shown in Fig. 3.1. The axisymmetric property of the geometry is conserved by adding the deformation to the entire circumference of the modified section. Figure 3.2 shows an example of the AXIE PANAIR mesh with a deformation added.

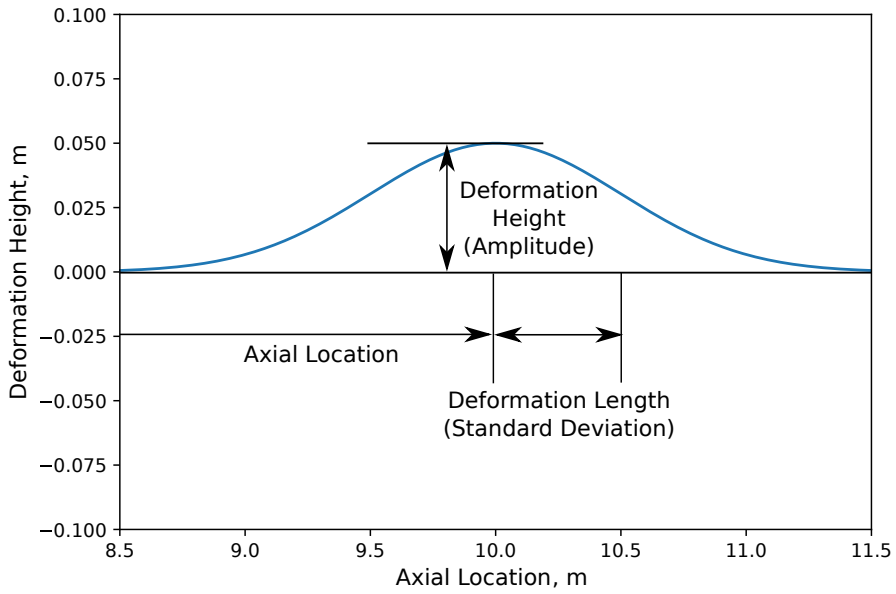

Fig. 3.1: Gaussian deformation description.

The design space is explored by analyzing all combinations of deformation parameters within a specified range. A range of positive and negative deformation heights as well as the axial locations are generated with a specified number of evenly spaced values. The

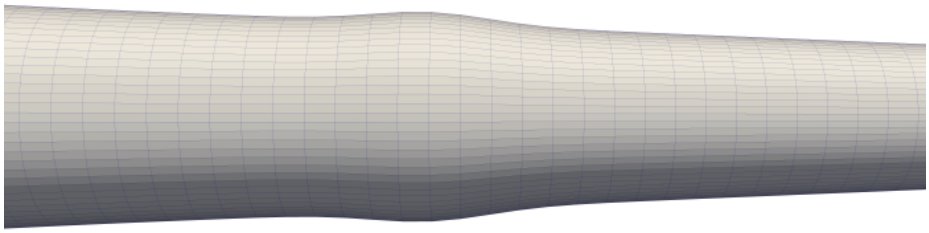

Fig. 3.2: PANAIR axisymmetric (AXIE) geometry mesh with positive deformation.

full combination of heights and locations are analyzed for a set deformation length and the resulting near-field signatures are propagated to the ground where the loudness of each is recorded. This analysis is performed for multiple deformation lengths until the design space has been explored to a desired level. To visualize the design space, the change in PLdB from the baseline AXIE PLdB for each deformation is mapped on a colored contour plot. These contour plots serve as a simple way to identify the locations and magnitudes of geometry changes that provide a reduction in PLdB.

3.2 Equivalent-Area Distribution - Discrete Deformations

As discussed previously, the near-field pressure disturbances of a body in linearized supersonic flow are affected by the lift and cross-sectional area distribution of the body. The superposition of these two contributions result in the total equivalent-area distribution. The relationship between the equivalent-area distribution, the near-field pressure disturbances, and the Whitham F-Function can be used to extend the concept of the equivalent area to capture higher-order flow effects. This work will utilize this relationship in the form of Eq.(3.1) which has been discussed previously but is presented here for convenience.

$$A_{E,r}(x) = 4\frac{\left(2R\sqrt{M_\infty^2 - 1}\right)^{\frac{1}{2}}}{\gamma M_\infty^2} \int_0^x \frac{\Delta p}{p_\infty}(t - x_0)\sqrt{x - t}\, dt, \tag{3.1}$$

In this work, the near-field signature for the NASA 25D has been generated for different flight conditions using a full Euler CFD solution. Additional near-field signatures from the

2017 2nd AIAA Sonic Boom Prediction Workshop are also used. These near-field signatures are converted to equivalent-area distributions using a code based on Eq.(3.1) [2]. This method allows for results that more closely couple the high and low-fidelity methods being used in the ULI.

The discrete deformation equivalent-area method is implemented in a manner similar to the AXIE method in exploring the design space. The equivalent-area distribution is modified with a similar parameterized Gaussian deformation. The height of the deformation represents the amplitude of the change in area and the length of the deformation is the range over which the change influences the area distribution. Figure 3.3 shows the variation in the equivalent area achieved by adding a Gaussian deformation to the original distribution. The design space is explored in the same way as the AXIE, with each study determined by a deformation length with varying deformation height and location. Contour plots are generated for the difference in PLdB from the baseline for comparison.

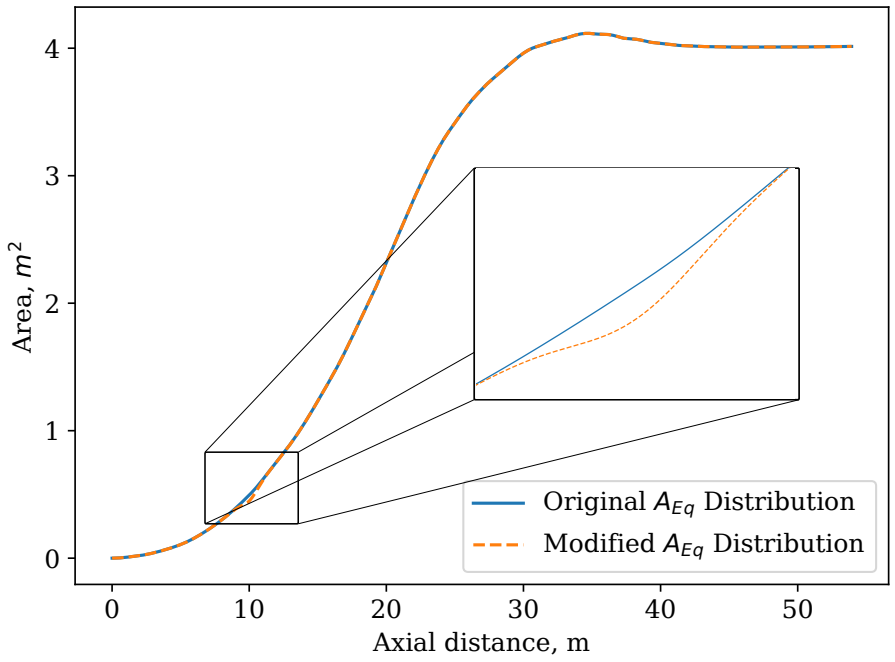

Fig. 3.3: Modified and unmodified equivalent-area distributions using the discrete deformation method.

[2] https://github.com/usuaero/rapidboom

Additionally, the discrete deformation method is used to study the effects of different atmospheric profiles on optimal deformations. Throughout the current work, the term optimal refers to the most effective deformations identified using the techniques outlined rather than a solution found using typical optimization computational guarantees. In this study a genetic algorithm (GA) known as the predictive parametric Pareto genetic algorithm (P3GA) is used [33]. This algorithm is a tool available through the ULI and has the functionality to run parametric optimization studies. In the scope of the current work, these parametric optimization tools are not used and thus the algorithm is more inline with a simplified GA method similar to NSGA-II [34]. A genetic algorithm is well suited for the problem at hand due to the likelihood of the existence of many local minimum and the black box nature of the sonic boom loudness tools used. Details of the problem formulation used with P3GA are included in the discrete deformation results section.

3.3 Equivalent-Area Distribution - Continuous Deformations

The continuous deformation equivalent-area method expands on the approach used in the discrete deformation method. This method uses a continuous cubic spline that is defined by any number of nodes that are equally spaced in the axial direction of the equivalent-area distribution. The end points, here chosen to be the first point of the equivalent-area distribution and a point slightly behind the last location representing a physical slice through the aircraft, are specified to have a zero first derivative and zero second derivative condition at the first and last points respectively. Everywhere along the interior of the cubic spline is twice continuously differentiable, by definition. This cubic spline fills the same role as the discrete parameterized deformation in that it represents a deviation from the original equivalent-area distribution.

The cubic spline represents a continuous deformation to the equivalent area that can be changed by activating and modifying the $\mathbf{y}$ value, representing the change in area, of each node or some subset of nodes. Additionally, if desired, the total number of nodes or the way they are distributed can be modified. Figure 3.4 shows an example of the continuous deformation with only a small section of the nodes active.

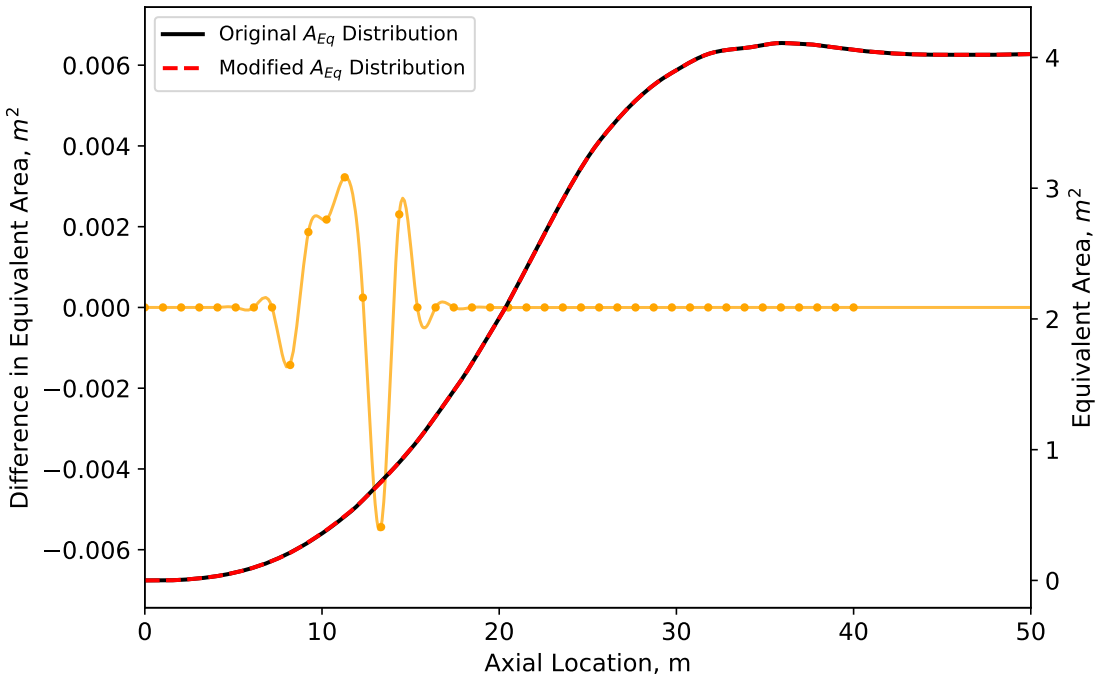

Fig. 3.4: Modified and unmodified equivalent-area distributions using the continuous deformation method.

The continuous deformation studies are done exclusively using a Python based gradient optimization tool [35]. Specifically, these studies utilize the SLSQP minimization method with constraints [36]. The optimization problem is formulated mathematically as follows:

$$\min_{\mathbf{y}} \sqrt{\frac{1}{N}\sum_{i=1}^{N}\left(A_{E,r}(x_i;\mathbf{y}_i) - A_{E,r}(x_i;\mathbf{y}_{i,0})\right)^2} \tag{3.2}$$

Subject to:

$$g(A_{E,r}(\mathbf{y}_i)) - g(A_{E,r}(\mathbf{y}_{i,0})) + \Delta PLdB_{goal} \leq 0$$

Where $g(A_{E,r}(\mathbf{y}_i))$ provides the total PLdB produced through running the sBOOM and PyLdB tools and $\mathbf{y}_i$ is the set of parameters representing deviations in the $\mathbf{y}$ value of the cubic spline mentioned previously. Essentially, the optimization method is used to minimize the change in equivalent area while matching some specified reduction in PLdB.

It is important to note that here the reduction in PLdB is set as a constraint and not as an objective function. This gives some flexibility in choosing what kind of solution is desired. Using this formulation, specific large or small PLdB goals can be set as well as a goal to simply return back to some baseline PLdB. Additional constraints used in this work are discussed in more detail in the continuous deformation results section.

The gradient based optimization approach outlined here allows for rapid study of different atmospheric profiles and different flight conditions. It is because of the lower computational load that the gradient based optimization is used with the more complex continuous deformation model.

3.4 Off-Design Flight Conditions

In an effort to identify more robust aircraft geometry changes for reducing sonic boom loudness, the equivalent-area methods outlined here are used to study a number of different off-design flight conditions. The aircraft flight variables considered in these studies are perturbations to Mach number, angle of attack, and azimuth angle. Atmospheric profiles with varying temperature, humidity, wind, and effective height above ground are explored as well. First, visual representations of the design space, as described previously, are used to identify locations and magnitudes of geometric aircraft changes most effective at reducing loudness. These visual representations help to formulate constraints within each of the optimization methods that have been discussed. Second, the discrete deformation method is used to study small changes in different atmospheric profiles. Lastly, the larger continuous deformation method is used to study the area changes required for larger reductions in PLdB at off-design conditions.

The use of the equivalent-area method provides a significant reduction in computation time. Because of this, the equivalent-area method is used for the bulk of the design space exploration. Specifically, the results for the standard atmospheric design condition are obtained using both the PANAIR AXIE and equivalent-area methods for comparison, while all off-design flight studies are done using the equivalent-area method alone.

The atmospheric profiles used in these studies are generated from weather measurements produced by the National Oceanic and Atmospheric Administration (NOAA)[3]. Related work that used the same process for generating atmospheric profiles was presented by Lazzara et al [37]. For the discrete deformation atmospheric studies, the profiles were pulled at a variety of latitude and longitude combinations for measurements taken on June 18, 2018. For the continuous deformation studies, the profiles were from atmospheric data sampled along a simulated flight path over the course of an entire year. These atmospheric profiles include distributions of humidity, temperature, and atmospheric winds which are all used as inputs to the NASA sBOOM code.

[3]This data is pulled directly from twisterdata.com, a website developed and maintained by David Demko and Donald Giuliano.

CHAPTER 4

DISCRETE DEFORMATIONS: PANAIR AND EQUIVALENT-AREA RESULTS

4.1 Standard Atmosphere

This work begins with exploring the effects of geometric changes to a supersonic aircraft in a standard atmospheric profile with no wind. The standard atmospheric profile is built into the NASA sBOOM code and defines a relative humidity for a given altitude [16]. The following studies are done using a cruise altitude of 45,000 ft (13.716 km). The results using the standard atmospheric profile provide a baseline for comparison in the proceeding studies.

4.1.1 AXIE Geometry Design Space Visualization

The AXIE design space is explored and visualized by analyzing cases for combinations of discrete Gaussian deformations over a range of heights, lengths, and locations. The range of axial locations includes 140 values from 0 to 50 m and the range of deformation heights includes 60 values between ± 0.05 m. The deformation lengths used are 0.125, 0.25, 0.5, 0.75, 1.0, 1.5, and 2.0 m. Figure 4.1 shows the design space using a Gaussian deformation with a length of 1.5 m where the contours show a change in PLdB from the baseline. Regions of blue indicate a reduction in PLdB and regions of red indicate an increase from the baseline.

Figure 4.1 shows minima at locations ranging from 12 m to 35 m. The minima at 12 m and 35 m are of particular interest and the deformation heights at these minima indicate that a reduction in the cross-sectional area is necessary to provide a reduction in PLdB. Plots of other deformation lengths show similar results but with varying degrees of PLdB reduction. Another cut through the design space can be visualized by varying deformation height and length while holding the axial location constant. The results shown in Fig. 4.2 show the minimum at a deformation length between 1.0 and 1.75 m. Figure 4.2 also shows

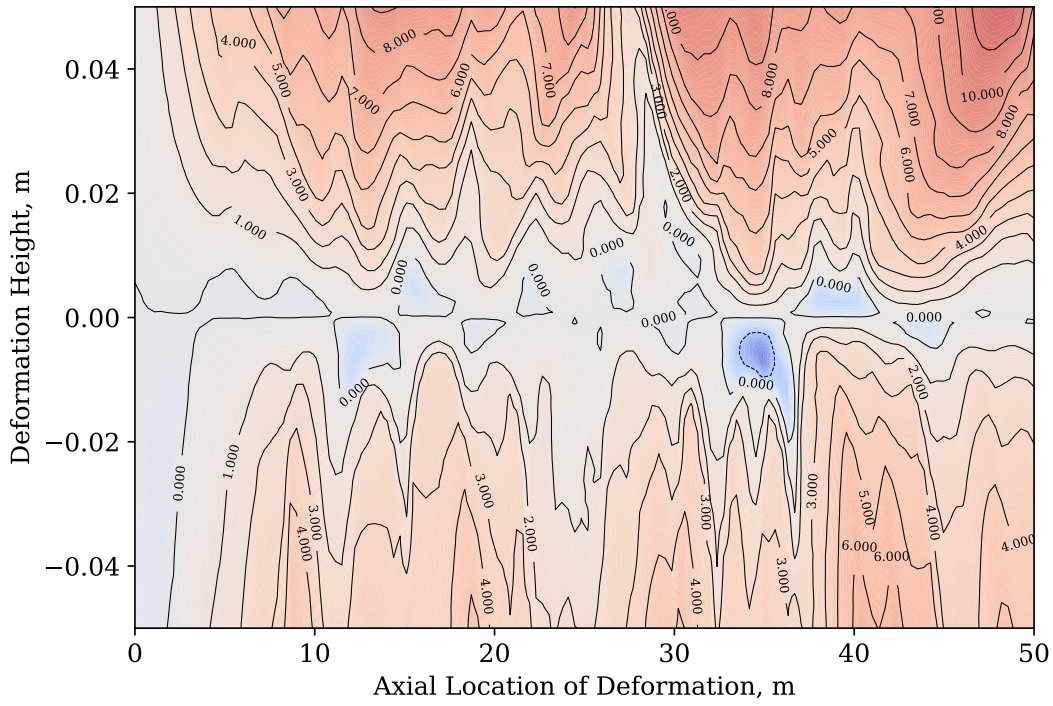

Fig. 4.1: Change in PLdB from baseline using AXIE model with a deformation length of 1.5 m.

that loudness is less dependent on deformation length than on height and location.

The minimum for the cases analyzed using the AXIE method was found to be a reduction of 1.73 PLdB for a deformation located at 34.89 m with a height and length of -0.0059 m and 1.5 m respectively. Figure 4.3 provides a visual representation of the full design space with the axes of the figure representing the different deformation parameters.

4.1.2 Equivalent-Area Design Space Visualization

The equivalent-area design space is visualized in the same way as the AXIE design space. The major difference between the two methods being that the equivalent-area distribution is modified and changed directly using the Gaussian function. The range of the Gaussian amplitudes is changed to ± 0.35 m^2 because it now represents a change in area rather than radius as in the AXIE method. Figure 4.4 shows the equivalent-area design space with the same 1.5 m deformation length as the AXIE plot (Fig. 4.1).

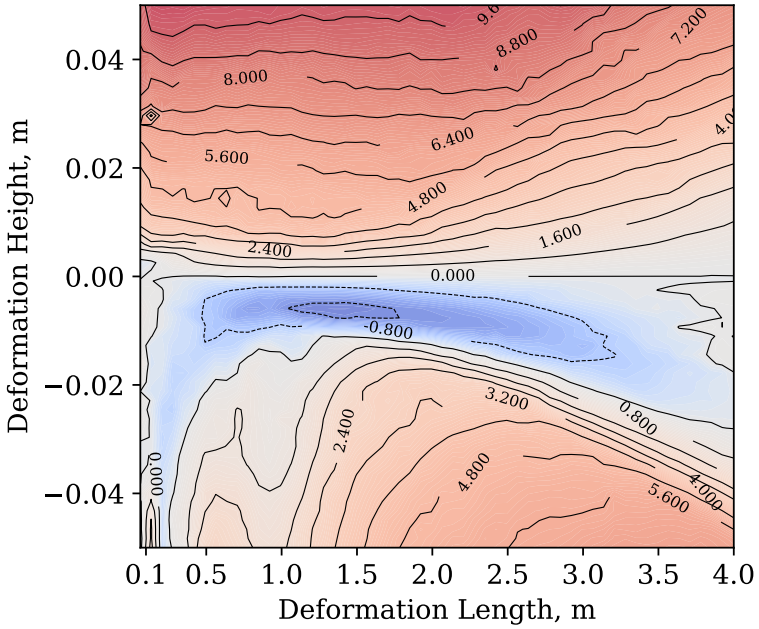

Fig. 4.2: Change in PLdB from baseline using AXIE model with an axial location of 35 m.

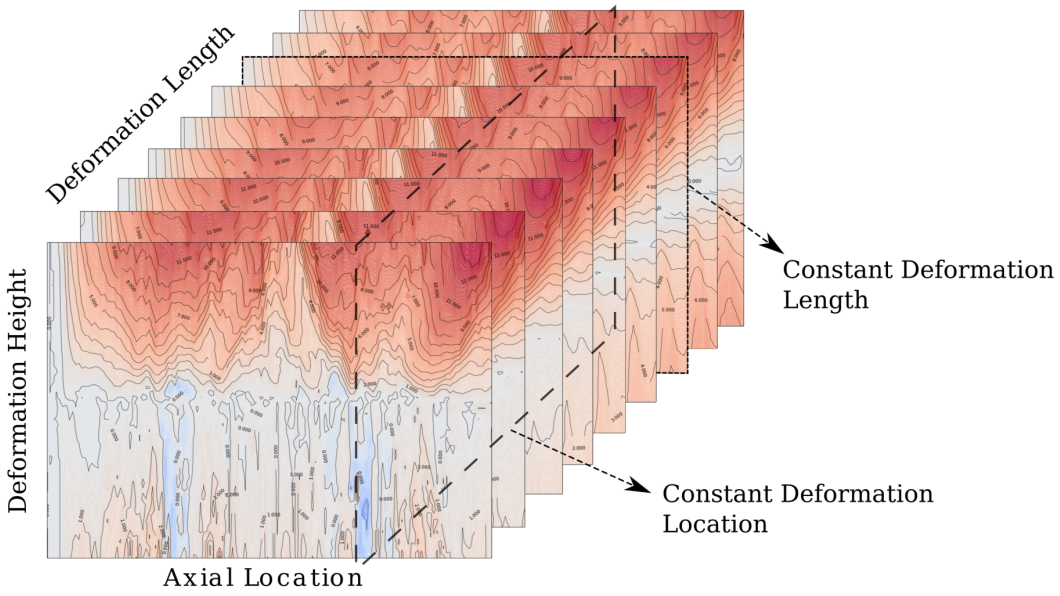

Fig. 4.3: Complete AXIE deformation design space.

There are similarities between the results of the equivalent-area method and those of the AXIE method. There are minima around the 12 m, 32 m, and 35 m locations, just as

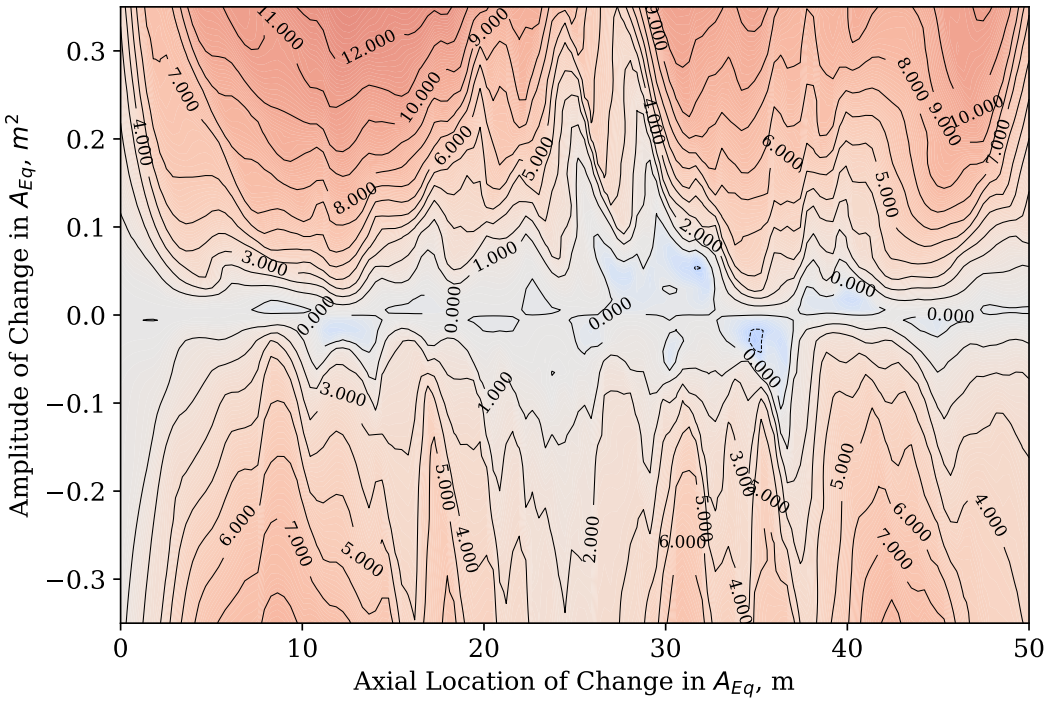

Fig. 4.4: Change in PLdB from baseline using the equivalent-area model with a deformation length of 1.5 m.

with the AXIE results. The equivalent-area method uses a slightly different approach than the AXIE method to explore this design space but, even though magnitudes of the minima are different, the similarities in locations and the other trends seen in the design space are very similar.

The goal of these studies is to provide locations and magnitudes of localized changes in geometry that are feasible for the actual aircraft geometry. This means that the results need to be constrained to magnitudes and locations that are feasible for the methods and techniques being used to accomplish the physical geometry changes. The design space exploration is useful as a first approach for gaining an understanding of the design space and, using these results, identifying realizable locations and magnitudes of geometry changes.

Figure 4.5 shows an equivalent-area design space for a Gaussian deformation with a 1 m standard deviation. An image of the NASA 25D with Mach lines is included for reference at the top of the figure. The minimum around the 12 m mark appears to correspond to the area

cut through the fuselage just before the wing. The minima at the 32 m mark correspond to the areas around the engine and the vertical and horizontal stabilizers. Locations further back than the 33 m mark correspond to area contributions from the vertical stabilizer and aircraft wake, which makes them difficult, if not impossible, to modify. Because of this, constraints used in the discrete deformation optimization studies are set to hold deformations to an axial location within 32.92 m (length of 25D). Deformation heights and lengths are also constrained to magnitudes between ±0.05 m and 0.125 m to 2 m respectively. These constraints were chosen as rough estimates of the ranges that would be considered feasible for adaptive aircraft structure design.

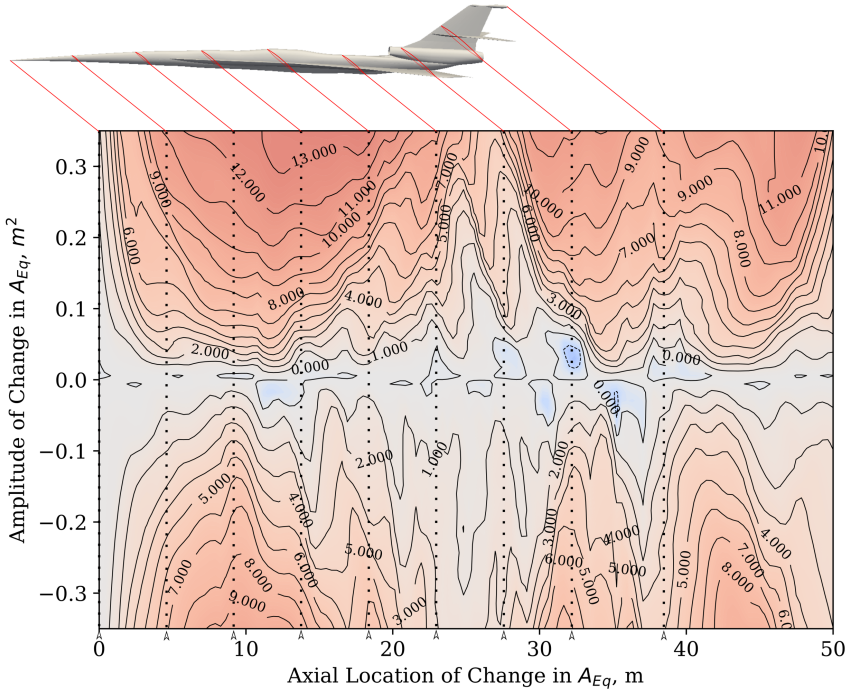

Fig. 4.5: Change in PLdB from baseline using equivalent-area model with physical representation of 25D aircraft for reference.

4.1.3 Optimization Benchmarking

In an effort to benchmark P3GA with the discrete deformation method, the AXIE method and P3GA are used together to identify the minimizing location, height, and length

variables for a deformation in the conditions and with the same constraints specified by the AXIE design space study. The P3GA solution is a deformation located at 35.04 m along the axis with a height and length of -0.0065 m and 1.30 m, respectively. This falls within the optimal basin seen in Fig. 4.1 and 4.2 for the AXIE design space exploration.

4.2 Historical Atmospheric Data: Optimization Using P3GA and Discrete Equivalent-Area Deformations

The following studies use the discrete deformation method and the genetic algorithm called P3GA. Here the design variables are the location, height, and length that define a Gaussian deformation. The objective is to minimize the total PLdB from an equivalent-area distribution in different atmospheric profiles. Details of the methods used for generating the atmospheric profiles and the genetic algorithm P3GA have been discussed previously. Constraints for the design variables were identified through the design space visualisation results and are used to maintain reasonable Gaussian deformations within this study. The mathematical formulation of this optimization problem is stated as thus:

$$
\begin{aligned}
&\Delta PLdB^* = [\min_{\mathbf{x}} F(\mathbf{x})] - PLdB_0 \\
&\text{Subject to:} \\
&\qquad g(\mathbf{x}) = \left| \frac{amplitude}{length} \right| \leq 0.02 \\
&\begin{bmatrix} 0 \\ -0.05 \\ 0.125 \end{bmatrix} \leq \begin{bmatrix} location \\ amplitude \\ length \end{bmatrix} \leq \begin{bmatrix} 32.92 \\ 0.05 \\ 2 \end{bmatrix}
\end{aligned}
\tag{4.1}
$$

where $\Delta PLdB^*$ represents the final change in perceived loudness, $PLdB_0$ is the perceived loudness of the unmodified equivalent-area distribution, and $\mathbf{x}$ is the vector of design variables specifying the *location*, *amplitude*, and *length* of each deformation. $F(\mathbf{x})$ represents the sBOOM and PyLdB tools used to produce the PLdB generated from a modified equivalent-area distribution. Problem (4.1) is solved to find the most effective deformation

for reducing PLdB in each atmospheric profile.

The results for the single deformation case are summarized in Table 4.1. Each of the final deformations are located near either the 12 m location or the 32 m location. These are the same locations that were identified as local minimums in the standard atmosphere design space visualization study. These results indicate that area should be removed in the 12 m location and added in the 32 m location, regardless of atmospheric profile.

Table 4.1: Most effective single deformation for multiple atmospheres.

		Deformation			
Latitude (°)	Longitude (°)	*Location* (m)	*Amplitude* (m^2)	*Length* (m)	$\Delta PLdB^*$ (dB)
34	-118	32.38	0.0198	0.992	-0.84
35	-112	32.39	0.0195	0.974	-1.01
36	-105	11.74	-0.0121	0.744	-0.82
37	-99	11.78	-0.0137	0.826	-0.78
38	-93	11.78	-0.0129	0.716	-0.82
39	-87	32.66	0.0153	0.766	-0.84
40	-80	32.35	0.0200	0.999	-1.03

The results in Table 4.1 show that the neither the 12 m or 32 m locations are best for all atmospheric profiles. While the reductions in loudness are all around 1 PLdB, there is a trade-off between the 12 m and 32 m locations being the most effective, depending on atmospheric profile. A study of what atmospheric properties might be dictating this exchange is a potential area of future work.

Next, the optimization is performed using two Gaussian deformations simultaneously. The results for this study are shown in Table 4.2. Again we see the combination of deformations around the 12 m and 32 m locations being found as most effective for each of the atmospheric profiles studied. Although the sample of atmospheric profiles is relatively small, these results suggest that the two locations identified near 12 m and 32 m should be primary locations of interest for deforming the full 25D geometry in higher-fidelity studies. These locations are shown relative to the full geometry in Fig. 4.6.

Table 4.2: Most effective simultaneous deformations for multiple atmospheres.

		Deformation 1			Deformation 2			
Latitude	Longitude	*Location*	*Amplitude*	*Length*	*Location*	*Amplitude*	*Length*	$\Delta PLdB^*$
(°)	(°)	(m)	(m^2)	(m)	(m)	(m^2)	(m)	(dB)
34	-118	11.77	-0.0118	0.722	32.27	0.0207	1.035	-1.88
35	-112	11.74	-0.0128	0.777	31.98	0.0167	1.061	-1.54
36	-105	11.77	-0.0098	0.723	28.37	0.0102	0.753	-1.27
37	-99	11.74	-0.0147	0.977	32.25	0.0204	1.021	-2.17
38	-93	11.82	-0.0130	0.772	32.33	0.0195	0.977	-2.03
39	-87	11.81	-0.0131	0.733	32.27	0.0204	1.021	-2.09
40	-80	11.96	-0.0146	1.307	32.31	0.0168	0.887	-1.78

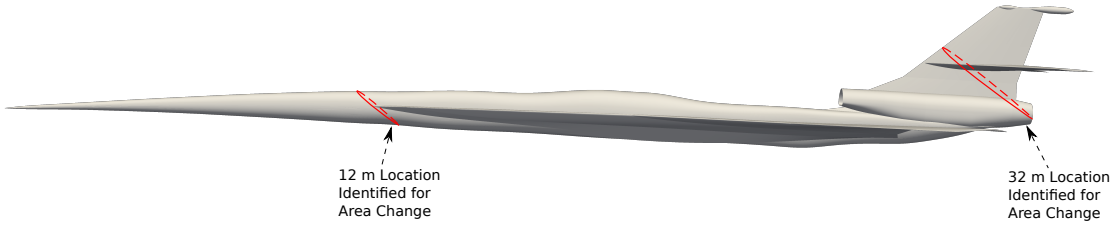

Fig. 4.6: Mach angle cuts of locations of interest identified on full 25D geometry.

4.3 Off-Design Flight Condition Sensitivity

An aircraft capable of changing its sonic boom signature during flight will be most useful if it can do so over a wide range of supersonic flight conditions. This study examines the effects of Mach number, angle of attack, and azimuth angle on the optimal deformations for reducing loudness. A brief study is done on how using an equivalent-area distribution from a powered CFD model versus an unpowered flow-thru model also affects the optimal deformations. Examining the effects of these conditions using the models previously built for the standard flight conditions allows for easy comparison. Near-field pressure distributions are found using Euler CFD solutions for the 25D at the varying flight conditions listed above. These pressure distributions are converted to equivalent-area distributions using the reversed equivalent-area code described previously.

In these studies, the discrete deformation equivalent-area method is used to explore the design space for each flight condition. This design space is the same as described in the standard atmosphere study where the three dimensions of the design space are the deformation location, height, and length. The PLdB is found for 90000 data points using 100 different axial locations, 30 heights, and 30 deformation lengths. The optimal equivalent-

area deformation for reducing loudness from the baseline for both the fore and aft locations of the aircraft, defined here as the front and rear half of the aircraft, are identified within the data points.

4.3.1 Mach Number

We first consider small perturbations in Mach number. The equivalent-area distributions for Mach number perturbations of ± 0.5 along with the on-design condition are generated from full Euler CFD solutions. All other flight parameters are held constant in a standard atmospheric profile at 50,000 ft (15.24 km). Figure 4.7 shows the amplitude, length, location, and resulting PLdB for the optimal fore and aft deformations.

The design space exploration results show that both the 12 m and 32 m locations remain optimal for each of the Mach numbers studied. The amplitude of the deformations at those locations are found to have very little sensitivity to deviations in Mach number. The length of the deformations show some variation at the lowest Mach number, but are otherwise consistent. Figure 4.7 also shows that PLdB is fairly sensitive to Mach number over the range studied. At a Mach number perturbation of -0.5 the fore location provides a greater reduction in PLdB than the aft location, which is opposite from all previous results. This indicates there is variation in the effectiveness of these deformations with respect to deviations in Mach number.

These results indicate that implementing structural adaptivity to change the equivalent area at both of these locations, 12 m and 32 m, remains a viable approach to reducing loudness, even with changing Mach number. The change in optimal location for the -0.5 Mach perturbation case indicates some variation exists in this range of Mach numbers and future work should focus on studying a larger range of Mach numbers with more intermediate Mach values.

4.3.2 Angle of Attack

The aircraft's angle of attack is the next off-design parameter studied. The equivalent-area distributions for angle of attack perturbations of $+0.2°$, $-0.4°$, and the on-design

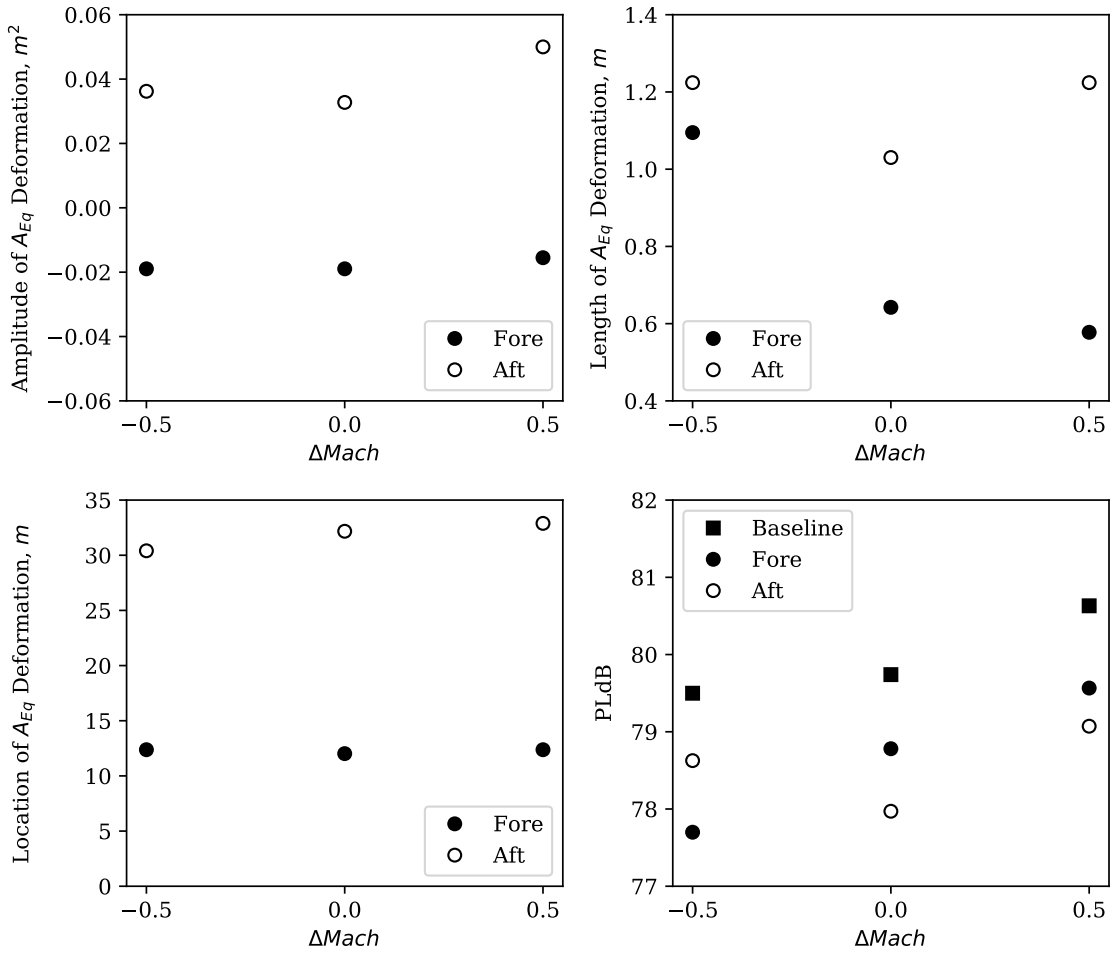

Fig. 4.7: Optimal deformation results vs. ΔMach.

condition are generated from full Euler CFD solutions. Figure 4.8 shows the resulting optimal fore and aft deformation parameters and loudness.

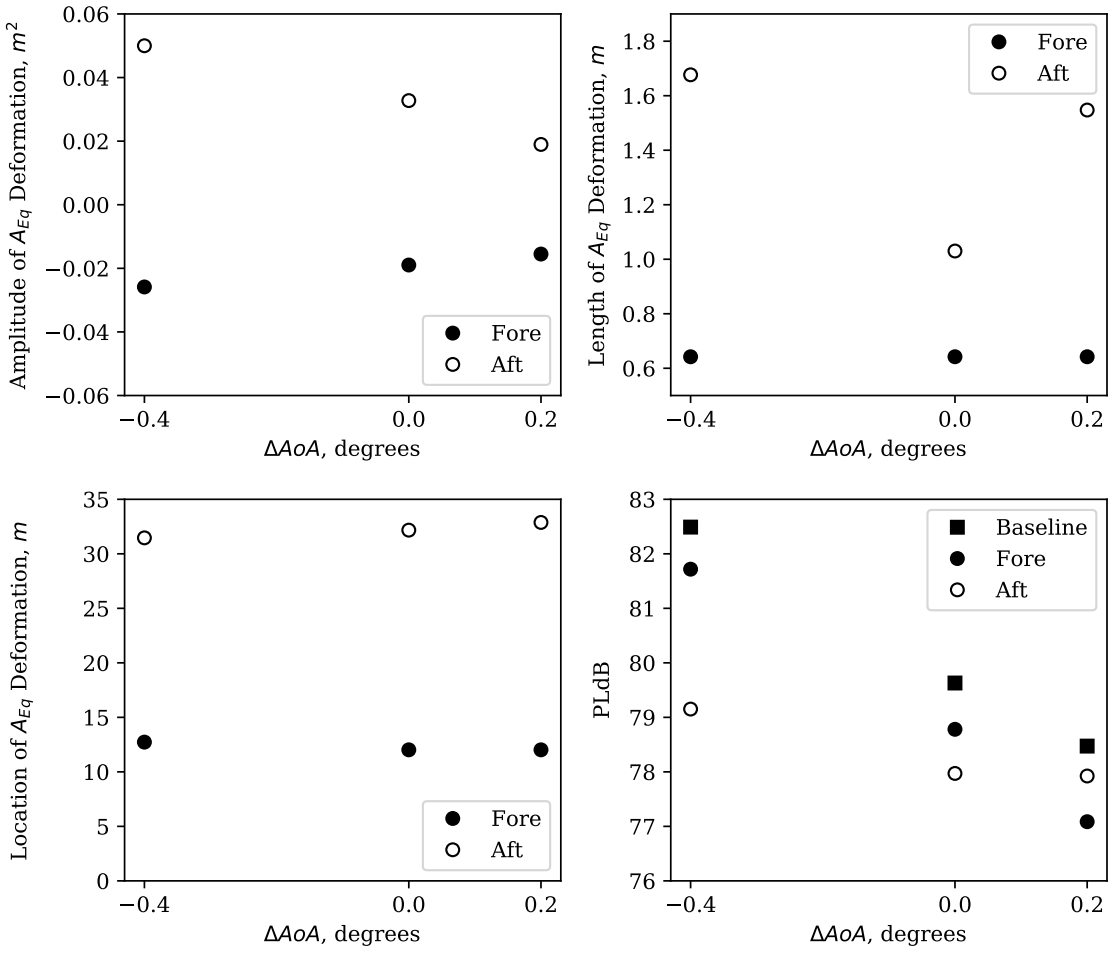

Fig. 4.8: Optimal deformation results vs. angle of attack.

The design space exploration results are similar to those seen in the Mach number and historical atmospheric studies. The amplitude and length of the aft deformations are far more sensitive to angle of attack than the the amplitude and length of the fore deformations. The optimal deformation locations appear to be insensitive to angle of attack. These results demonstrate that the optimal deformations have some dependence on angle of attack, but do not vary significantly from the on-design results.

Figure 4.8 also shows that the achievable loudness is sensitive to angle of attack. The aft location is optimal for both the on-design and smaller angles of attack but the optimal switches to the fore location for the larger angle of attack, similar to what was seen for a smaller Mach number. These results continue to support the trend of a bimodal optimum that demonstrates the fore and aft locations being necessary to recover from the increase in PLdB caused by these off-design flight parameters. Again, future work should focus on a larger and more populated range of angle of attack, which could provide more insight to the variations seen in the optimal deformation across the current range of angles of attack.

4.3.3 Azimuth Angle

Sensitivity to azimuth angle was also considered. The near-field signatures from Euler solutions for azimuth angles between 0° and 50° at 2° increments are converted to equivalent-area distributions. Figure 4.9 shows the azimuth angle as defined from the undertrack of the aircraft.

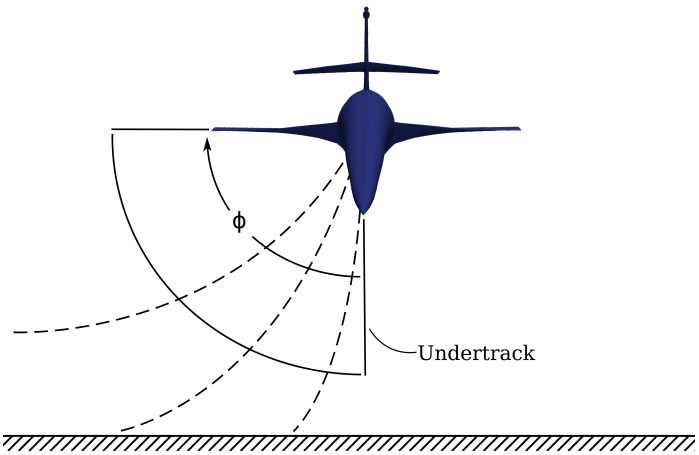

Fig. 4.9: Azimuth angle measured from the aircraft undertrack.

The optimal fore and aft deformations are identified and recorded using the same design space exploration methods described previously. Figure 4.10 shows the optimal deformation parameters as functions of azimuth angle for the fore and aft locations of the aircraft.

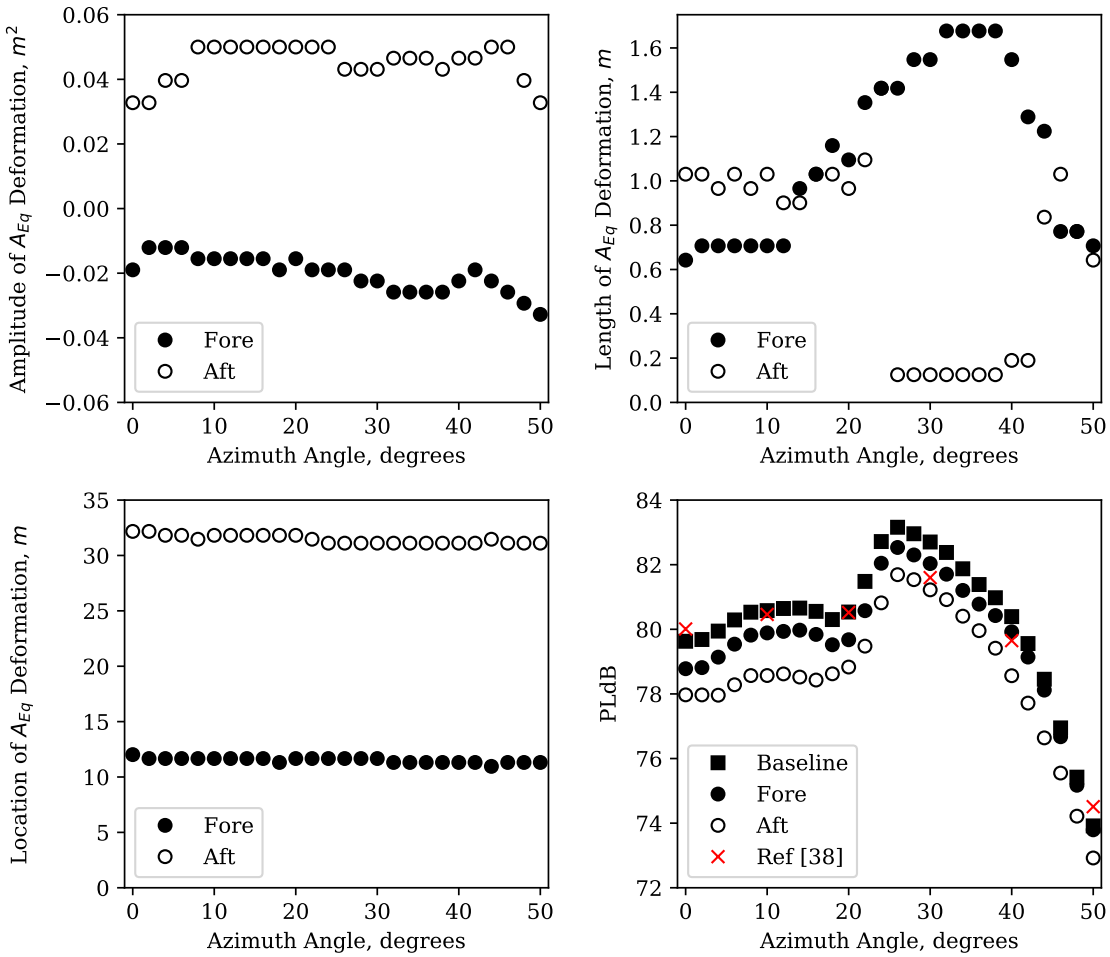

Fig. 4.10: Optimal deformation results vs. azimuth angle.

Figure 4.10 shows that the magnitudes and locations of the optimal deformation amplitudes are consistent with those seen in previous studies and are fairly insensitive to azimuth angle [38]. The length of these optimal deformations shows a large sensitivity to azimuth angle; although, we have seen that, for a standard atmosphere, the loudness produced is less sensitive to deformation length than the other parameters.

Figure 4.10 also shows large sensitivity to azimuth angles in the baseline and optimal PLdB produced using a fore and aft deformation. The maximum PLdB occurs from the near-field signature at an azimuth angle around 30° and an aft deformation always provides a larger reduction in PLdB from the baseline. The results in Figure 4.10 show consistency in the optimal location and amplitude of deformations but significant changes in length are necessary to meet that optimum for different azimuth angles.

4.3.4 Powered Model

One model that the Sonic Boom Workshop has additional results for is a powered aircraft with the engine plume. An equivalent-area model is created from the Workshop's near-field pressure signature of this powered aircraft and implemented in the design space exploration. The powered pressure signature is only available for on-design flight conditions. Therefore, the only comparisons that are made are to the unpowered on-design results.

Figure 4.11 shows loudness contours for the unpowered and powered models. A comparison of these plots shows some variations in the PLdB minima. The minimum at the fore location appears mostly unchanged while the aft minimum has shifted further back from the 32 m location. The baseline PLdB for the powered model is 81.10 PLdB, or about 1.5 PLdB greater than the unpowered model. The aft deformation on the powered model is able to produce a 1.58 decrease in PLdB from the baseline, down to 79.52 PLdB, while the aft deformation on the unpowered model produces a 1.66 decrease in PLdB, down to 77.97 PLdB.

Ideally, future work would incorporate more use of the powered model at the different flight conditions examined thus far. The results of the baseline powered and unpowered model comparison show the aft deformation shifting further back on the aircraft, to some-

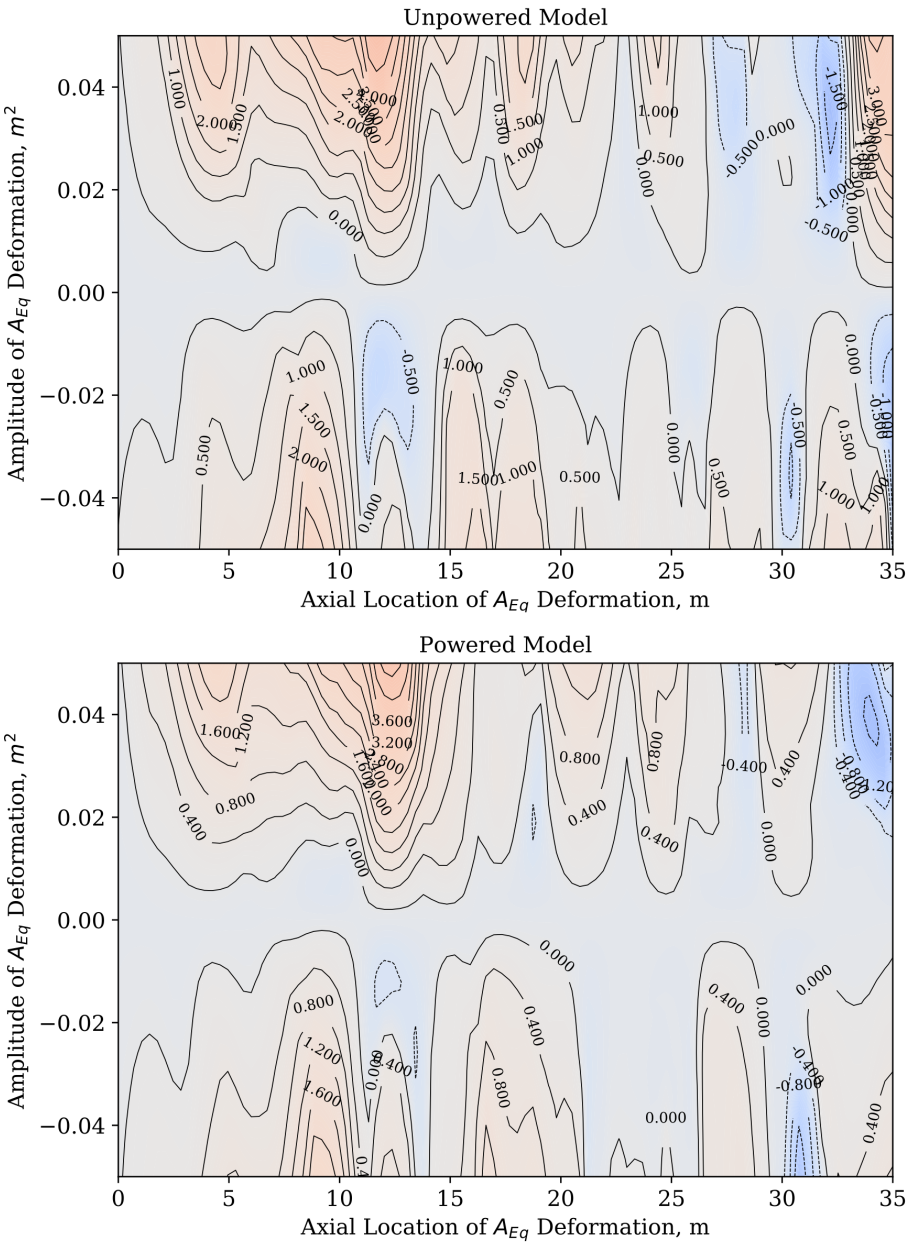

Fig. 4.11: Change in PLdB from baseline using equivalent-area model for unpowered and powered 25D with deformation lengths of 1.03 and 1.16 m respectively.

where on the vertical stabilizer. These results are still useful for informing the higher fidelity studies with locations of interest to deform the full three-dimensional geometries.

4.4 Summary of the Discrete Deformation Studies

The results of the discrete deformation studies have continuously shown the locations of 12 m and 32 m to be the most effective at reducing the loudness of the 25D. This results holds true even when considering different atmospheric profiles and a small range of off-design flight conditions. Efforts to modify the more complex 3D configurations of the 25D for use in CFD studies should begin with these two locations. The process used for solving the inverse design problem of generating a 3D geometry that matches a modified equivalent-area distribution is demonstrated in the work by Weaver-Rosen et al [29]. In this work, the authors use an approach very similar to what has been done here to generate a target modified equivalent area which helped reduce the CFD results down to a handful of candidate solutions. The results presented in this discrete deformation equivalent-area section have been published previously here [39].

CHAPTER 5

CONTINUOUS DEFORMATIONS: EQUIVALENT-AREA RESULTS

This section utilizes the continuous spline deformation outlined in the computational methods section of this thesis. These studies look to further explore the changes to an aircraft's equivalent-area distribution that are required to reduce its sonic boom loudness at a variety of off-design conditions. As in the discrete deformation studies, the equivalent-area changes required to reduce PLdB for a number of atmospheric profiles and small perturbations in Mach number and angle of attack are sought. These efforts are expanded by looking at a few cases of combined Mach and angle of attack changes in a standard atmosphere as well as in adverse atmospheric profiles.

The studies presented in this section utilize the same standard atmospheric profile as described previously. A slightly larger altitude of 50,000 ft (15.240 km) is used in these continuous deformation studies compared to the 45,000 ft used in the design space visualization studies. This change in altitude was implemented to better align with the CFD work and atmospheric profile studies that had been completed within the ULI between the completion of the discrete deformation studies and the beginning of the current studies. This change should have relatively little impact on the final solutions as it is the difference in sonic boom loudness and not the total loudness that is of most interest in the current work.

5.1 Deformation Method Comparison

Although the discrete and continuous deformation methods have been described previously, a visual comparison of the two methods will help orient the reader to the differences. Figure 5.1 shows two solutions that achieve a 1 PLdB decrease for the 25D in a standard atmosphere and at on-design flight conditions. The blue curve shows a symmetric discrete

deformation at the 12-13 m location, similar to what has been identified as a location of interest in previous studies. The orange curve is a continuous deformation solution that was only active between the 7-16 m region. These solutions have some obvious similarities and differences. The continuous solution shows a decrease in area in nearly the same location as the discrete deformation, although the magnitude in area change as well as the length that this particular decrease in area occurs over are both smaller. The continuous solution shows additional regions of area change immediately before and after the 12 m decrease which is not possible using the discrete deformation method. This comparison demonstrates the advantage of the continuous deformation in a achieving larger and more varied changes to the equivalent-area distribution. It is these larger changes that allow for greater reductions to the sonic boom loudness.

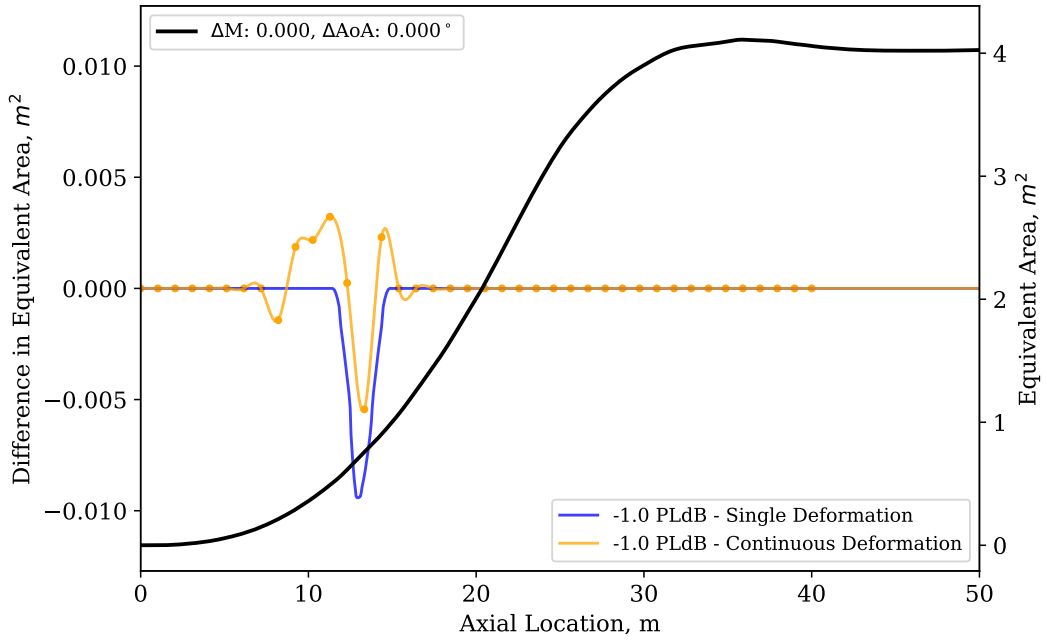

Fig. 5.1: Equivalent-area deformation method comparison using 1 PLdB solutions.

5.2 Standard Atmosphere

One goal proposed by the ULI at its onset was to achieve loudness reductions of up to 5 PLdB. The discrete deformation studies showed that small single or double deformations were only able to achieve reductions of about 2 PLdB. To explore the feasibility of this larger PLdB reduction goal, a constraint of a 5 PLdB reduction is used in the gradient optimization tools for the initial continuous deformation studies. The spacing of the cubic spline nodes are chosen to strike a balance between computational time and the length of individual deformations that could be represented. For the studies presented here, a spacing of approximately 1.482 m is used between each node which provides a total of 28 nodes across the 40 m length of the full spline. Only nodes between 0 and 36 m are active, resulting in 24 active nodes, and a constraint of $\pm 0.075\, m^2$ is placed on the allowable vertical displacement of the nodes. This effectively constrains changes to the equivalent area to the regions associated with the Mach plane slicing of the physical aircraft and limits the magnitude of changes to be within the effective range identified in the discrete deformation studies. It is worth noting that these constraints represent a slight relaxation on the constraints used in the discrete deformation studies. The axial locations that the area that can now be modified include the region of the vertical stabilizer and the magnitude of allowed changes are slightly larger. These changes are made to allow for larger deformations capable of achieving the necessary changes in PLdB.

Figure 5.2 shows a continuous deformation solution for a 5 PLdB reduction in the standard atmospheric profile. The familiar decrease in area around the 12 m location and increase in area around the 33 m location are present. Additional features, such as the gradual increase in area at the front of the distribution, stand out but all changes seem well defined over the length of the aircraft.

5.3 Atmospheric Profiles From a Simulated Flight Path

An additional goal of the ULI was to simulate the loudness reducing adaptive structures for an overland supersonic flight across the United States. A separate ULI team performed a range of atmospheric profiling studies and chose Seattle, Boise, Denver, Dallas, and Miami as

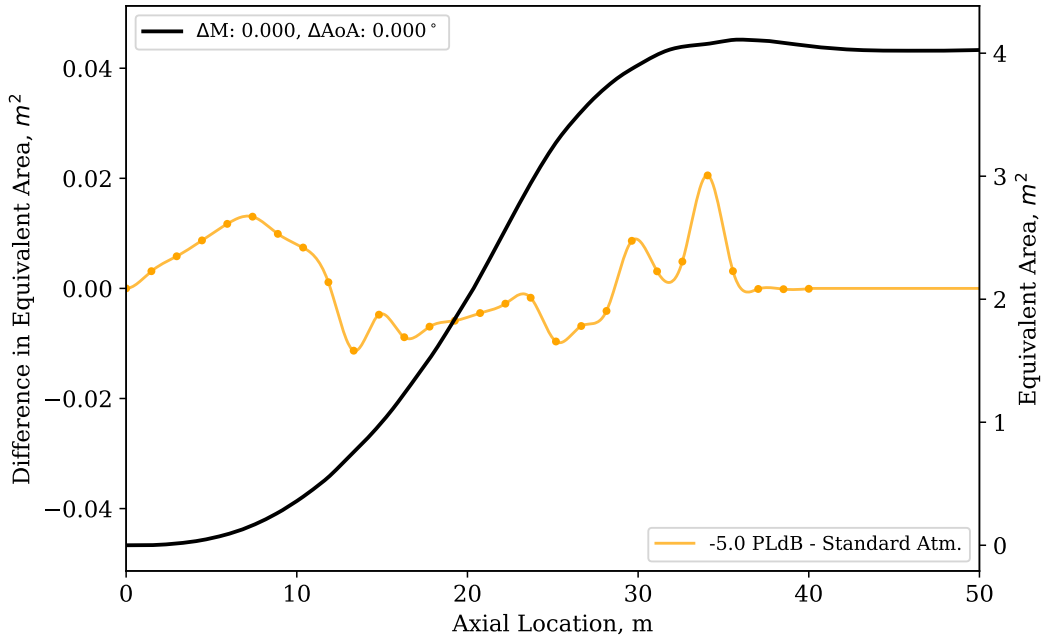

Fig. 5.2: Continuous deformation solution for a 5 PLdB reduction in the standard atmosphere profile at on-design flight conditions.

locations along a flight path to sample atmospheric profiles. Figure 5.3 shows the simulated flight path. The source of the atmospheric data analyzed was discussed previously. The profiles chosen were worst-case scenarios for PLdB at these locations from data sampled over the course of a year. The baseline PLdB for the 25D in these atmospheric profiles can be seen in Table 5.1. While the deviation from the standard atmosphere PLdB for these 5 atmospheric profiles is relatively low, it is still desirable to see how the necessary deformations to an equivalent-area distribution might change.

A 5 PLdB constraint is again implemented in the gradient optimization tools. The same constraints on the range of active nodes and the magnitude of allowable deflection that were used in the standard atmosphere continuous deformation study are also used here. Figure 5.4 shows the solutions for the different atmospheric profiles used. With the exception of the Boise profile, all cases achieved a 5 PLdB reduction.

The front portion, including the gradual increase in area followed by the sudden decrease in area, and the aft portion, including the a sudden increase around 33 m, match

Fig. 5.3: Locations of atmospheric profiles sampled along a simulated flight path.

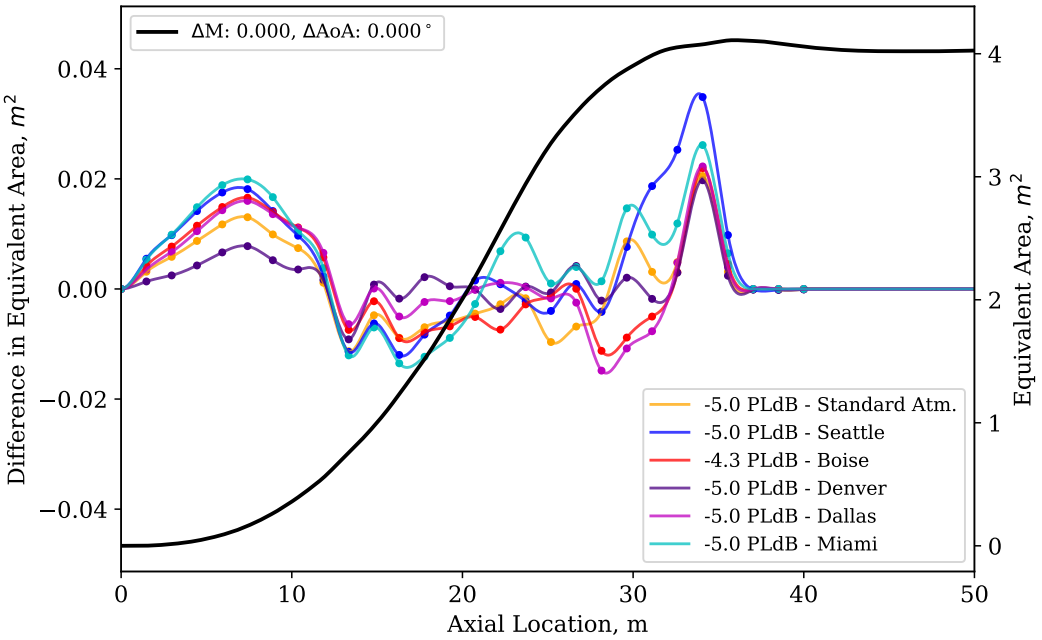

Fig. 5.4: Continuous deformation solutions for a 5 PLdB reduction in different atmospheric profiles at on-design flight conditions.

closely with the standard atmospheric solution. The solutions show the same decrease in area around 12 m and increase in area around 33 m that has been seen in multiple previous studies. While some signatures share a few common features in the center portion of the solution, between 12 m and 33 m, there are no consistent and recognizable features between all solutions in this region. It is interesting to note that the features common among all solutions show a difference in magnitude dependent on atmospheric profile. This is most obvious in the gradual rise at the front of the solutions and may suggest that similar deformations might be applicable in each profile and that only varying levels of deformation magnitude are necessary to achieve the desired loudness reduction.

5.4 Off-Design Flight Conditions

This section looks to study the effects of off-design Mach number and angle of attack using the continuous deformation method. Like in the off-design studies of the discrete deformation method, each off-design case requires an Euler CFD solution to generate the new equivalent-area distribution. It is for this reason that only a few cases of off-design Mach number and angle of attack are examined. Each of these off-design cases is ran using the standard atmospheric profile with the same constraints to node location and displacement magnitude as the previous continuous deformation studies. One major difference here is instead of the arbitrary 5 PLdB reduction goal these studies will simply look to return the PLdB back to the level of the 25D in a standard atmosphere at on-design flight conditions. It is worth noting that the on-design equivalent area for the NASA 25D used here is slightly different than the one used in the discrete deformation studies. This results in a slightly lower baseline PLdB than previously shown. This change is a result of changing responsibilities within the ULI and the new equivalent-area distribution is one that matches the most current CFD work being done. A summary of the off-design values and results can be found in Table 5.1.

5.4.1 Mach Number

The Mach number cases that are studied here are the same as those studied in the discrete deformation studies which included small perturbations of ±0.5 to the baseline Mach number of 1.6. Figure 5.5 shows the original equivalent-area distributions as well as the deformation solution for each Mach number case. The 5 PLdB standard atmosphere solution is included for reference.

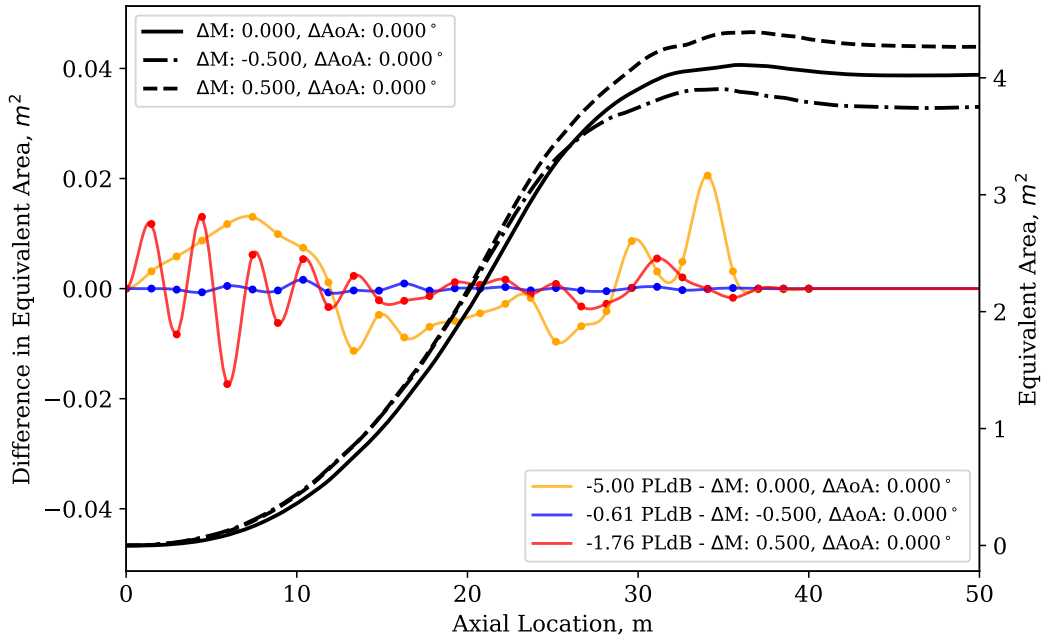

Fig. 5.5: Continuous deformation solutions for off-design Mach number in a standard atmosphere.

In each case the change in PLdB from the on-design standard atmosphere was recovered, although the solutions here are drastically different from what have seen previously. In the $\Delta M = -0.500$ case the required change in loudness was small as was the deformation required to recover it. The change in PLdB for the $\Delta M = 0.5$ case was larger and the resulting solution includes a region of rapid area change at the front of the distribution and a single larger positive deformation at the rear of the distribution around the 31 m mark. Both solutions suggest that the front of the distribution is more sensitive to area change

than has been seen in previous studies.

5.4.2 Angle of Attack

The angle of attack cases that were studied in the discrete deformation section included perturbations of $+0.200°$ and $-0.400°$. Those cases are also used here in the continuous deformation study but for the $+0.200°$ case the resulting PLdB in a standard atmosphere is lower than the on-design case. For that reason, Fig. 5.6 only shows the solution for the $-0.400°$ case. The original equivalent-area distributions are included for each of the off-design cases.

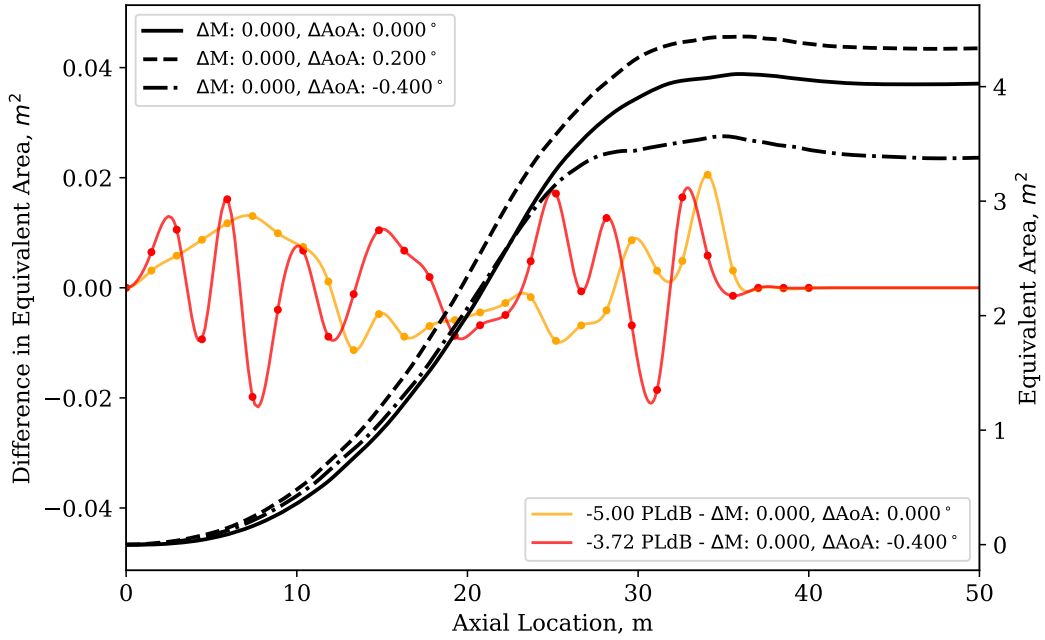

Fig. 5.6: Continuous deformation solutions for off-design angle of attack in a standard atmosphere.

The $-0.400°$ solution was able to recover the full 3.72 PLdB deviation from the on-design case. This solution shows the front part of the distribution requiring similar oscillations in area deformation to what was seen in the Mach number study. There are a few regions of more notable area changes such as the increases in area between 11 and 18

m and between 23 and 30 m and the large decrease in area at the 31 m location. There are no obvious similarities between this solution and any of the previous studies and it is difficult to say what areas of the continuous deformation have the most impact on the total PLdB change. This solution suggests that almost the entire length of the area distribution is sensitive to area change.

5.4.3 Combined Mach Number and Angle of Attack

The final study using a standard atmospheric profile looks at cases of simultaneous perturbations to Mach number and angle of attack. The first case is for a -0.017 perturbation to Mach number and a $-0.273°$ perturbation to angle of attack. The second case is for a $+0.071$ perturbation to Mach number and a $+0.392°$ perturbation to angle of attack. Figure 5.7 shows the original equivalent-area distributions for each case as well as the optimal continuous deformation solutions.

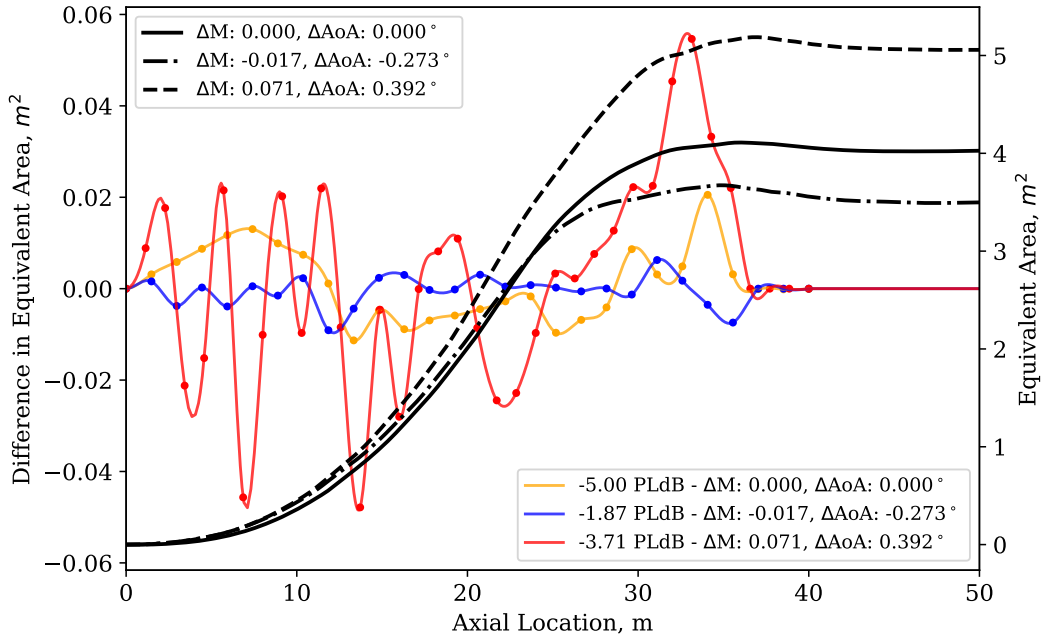

Fig. 5.7: Continuous deformation solutions for off-design Mach number and angle of attack in a standard atmosphere.

For the first case the total deviation in PLdB was recovered but for the second case only 3.71 PLdB of the 4.66 PLdB deviation was recovered. The first case shows that relatively small deformations to the equivalent area are necessary to recover the deviation in PLdB. The front portion of the equivalent-area distribution seems to be the most sensitive to area change with the exception of the 30 - 35 m range also being sensitive. The second case shows that large deformations to the equivalent area are necessary to recover the deviation in PLdB. The oscillations at the front of the distribution are again present but with much larger magnitudes in this case. This solution also shows a large increase in area is necessary at the rear of the distribution. This increase in area appears to be the largest required deformation seen yet.

5.5 Combined Off-Design Flight Conditions in Adverse Atmospheric Profiles

The final study done using the continuous deformation method looks at the optimal equivalent-area changes for reducing PLdB for both off-design flight conditions combined with adverse atmospheric profiles. The four cases examined here look at the same combination of off-design flight conditions as the previous study and each of those within the Boise and Denver atmospheric profiles. These cases represent the culmination of conditions considered in the current work that can degrade a sonic boom's loudness. Table 5.1 again summarizes the results of these studies.

Figure 5.8 shows the optimal deformations for the first off-design case of a -0.017 perturbation to Mach number and a $-0.273°$ perturbation to angle of attack as well as the second off-design case of a $+0.071$ perturbation to Mach number and a $+0.392°$ perturbation to angle of attack. Both of these cases are ran using the Boise atmospheric profile.

The first case was able to recover the full deviation in PLdB caused by the off-design and atmospheric conditions. This solution shows sensitivity in the front of the distribution in a manner similar to the standard atmosphere solution, but with a larger negative deformation around the 12 m location. Additionally, this solution shows sensitivity at the 25 m and 31 m locations that require an increase in area. The deformations at 12 m and 31 m are similar to the ones seen for this off-design case in the standard atmosphere solution.

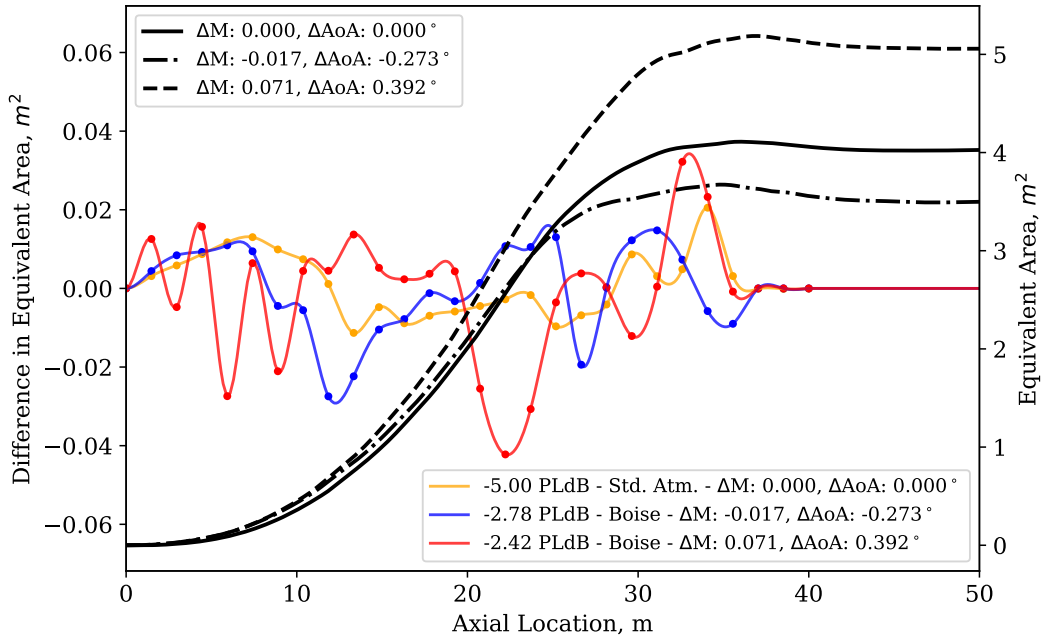

Fig. 5.8: Continuous deformation solutions for off-design Mach number and angle of attack in the Boise atmospheric profile.

The solution for the second case was only able to recover 2.42 PLdB of the 3.91 PLdB deviation. This solution shows similar sensitivity at the front of the distribution to what has been seen previously for this off-design case. The large negative deformation at the 22 m location as well as the positive deformation at the 33 m location are also very similar to the ones seen in the standard atmosphere solution for this off-design case.

Figure 5.8 shows the optimal deformations for the same off-design cases within the Denver atmospheric profile. The first case was able to recover the full 2.72 PLdB deviation. This solution shows the same sensitivity at the front of the distribution as was seen in the Boise solution. The rear of the solution also appears sensitive to area change but with different optimal deformation features than were seen in the Boise solution. The second case was only able to recover 1.85 PLdB of the 4.41 PLdB deviation. The second case shows a different deformation pattern at the front of the distribution and the rest of the solution seems significantly different from the Boise solution.

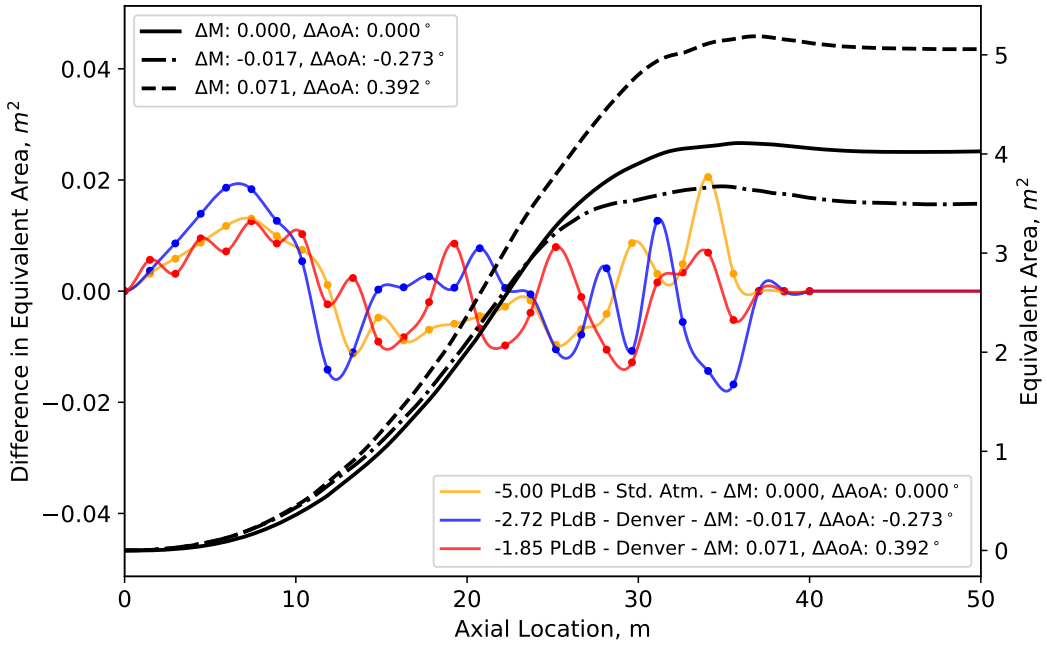

Fig. 5.9: Continuous deformation solutions for off-design Mach number and angle of attack in the Denver atmospheric profile.

5.6 Summary of the Continuous Deformation Studies

Each of the solutions presented in this section show that deformations distributed over the entire length of the aircraft are necessary to achieve the specified reductions in PLdB. This strengthens the case for distributed OML adaptivity proposed by the ULI. While most of the deformations shown in these solutions are of relatively small magnitude (less than $0.06\,m^2$) the frequency and length over which these deformations occur may pose problems to a CFD team trying to model these deformations on the full aircraft and also to those responsible for designing the actuators themselves. Because of this, an area of future work would be to post-process and refine the results shared here to identify the regions of greatest sensitivity to area change. An alternative approach that would accomplish the same goal is to systematically confine the continuous deformations to smaller areas of the equivalent-area distributions and run multiple cases for each off-design condition. This would essentially be finding a balance between the continuous deformation solutions shown here and the discrete deformation solutions shown previously.

It is also important to note that the use of gradient optimization tools in this application is likely to yield only a local minimum in a design space as complicated as the one being studied here. Because of this, the solutions shown here are primarily useful for identifying regions of sensitivity that should be explored using higher fidelity tools rather than assuming the solutions found are absolute minimums themselves.

Table 5.1: Summary of optimal continuous deformation atmospheric and off-design studies.

ΔMach	ΔAoA	Atmosphere	Baseline PLdB	ΔPLdB From On-Design	ΔPLdB Achieved
0.000	0.000	Standard	78.76	-	-5.00
Atmospheric Study - 5.0 PLdB Goal					
0.000	0.000	Seattle	79.34	0.58	-5.00
0.000	0.000	Boise	79.52	0.76	-4.31
0.000	0.000	Denver	79.43	0.67	-5.00
0.000	0.000	Dallas	78.77	0.01	-5.00
0.000	0.000	Miami	78.23	-0.53	-5.00
Mach Study - Std. Atmosphere Baseline 25D Goal					
-0.500	0.000	Standard	79.37	0.61	-0.61
0.500	0.000	Standard	80.52	1.76	-1.76
AoA Study - Std. Atmosphere Baseline 25D Goal					
0.000	0.200	Standard	78.47	-0.29	N/A
0.000	-0.400	Standard	82.48	3.72	-3.72
Combined Off-Design Study - Std. Atmosphere Baseline 25D Goal					
-0.017	-0.273	Standard	80.63	1.87	-1.87
0.071	0.392	Standard	83.42	4.66	-3.71
-0.017	-0.273	Boise	81.52	2.76	-2.78
0.071	0.392	Boise	82.67	3.91	-2.42
-0.017	-0.273	Denver	81.48	2.72	-2.72
0.071	0.392	Denver	83.17	4.41	-1.85

CHAPTER 6

SUMMARY OF RESULTS AND CONCLUSION

Low-fidelity equivalent-area methods were used to explore the design space of localized geometric changes to the NASA 25D's OML. The geometric changes were used to alter the aircraft's near-field pressure signature in a way that reduced its sonic boom's loudness at the ground. Initially, discrete deformations were made to an axisymmetric PANAIR model and the 25D's equivalent-area distributions. The equivalent-area method design space was shown to have the same minima as the alternative PANAIR design space. The design space exploration was used to identify locations on the aircraft's geometry that can be modified to minimize PLdB. Locations at 12 m and 32 m on the NASA 25D concept aircraft show the most promise for reducing loudness.

A genetic algorithm called P3GA was used to study the effects of varying atmospheric profiles on the optimal discrete deformations required to minimize PLdB. The locations of 12 m and 32 m were again found to be the areas most effective for reducing loudness on the undertrack. With two deformations used, the maximum reduction in PLdB was found to be -2.17.

The discrete deformation equivalent-area design space exploration was also used to study the effects of small perturbations to on-design flight conditions. The optimal deformations for changes in angle of attack, Mach number, and azimuth angle were found. The off-design results show the locations and magnitudes of the deformations remain consistent. There is some variation in which deformation produces the greatest PLdB reduction, but the minimums remain at the 12 m and 32 m locations. The use of a powered aircraft model was shown to shift the aft minimum slightly further back.

A larger continuous deformation was used to study the changes to the aircraft's equivalent area that are required to achieve even larger reductions in PLdB. The continuous

deformation studies began with a 5 PLdB goal in the standard atmosphere and in atmospheric profiles representing a simulated flight path. In each case, the 12 m and 32 m locations were again identified within the solutions as regions of sensitivity.

The continuous deformation studies were extended to study small perturbations to Mach number, angle of attack, and combinations of both within a standard atmospheric profile and few of the flight path profiles. These studies used the goal of returning the off-design PLdB back to the PLdB of the baseline 25D in a standard atmosphere. The results of these studies show that extensive distributed deformation along the length of the area distributions are necessary to recover the deviations in PLdB and in some cases fall short of that goal. A few common areas of sensitivity were identified through these studies for specific off-design conditions. These results lack significant similarities across all off-design and atmospheric conditions which suggests that additional refinement of the method or solutions is necessary. Future work could involve systematically confining the continuous deformation method to specific regions along the aircraft's area distribution. This work would essentially be a combination of the discrete and continuous deformations presented here and would help narrow down the regions of interest for the larger PLdB reduction goals. Additionally, the inconsistency and complexity of these results may simply be due to the complexity of the design space that was being explored.

While the equivalent-area representation does not provide an exact mapping of a deformation back to a three-dimensional aircraft geometry, the current work has shown how it can be used to narrow down the design space for higher fidelity CFD studies. These results are also useful within the ULI for informing preliminary design steps to the individuals designing the adaptive aircraft structures themselves. The equivalent-area methods shown here can drastically reduce the computational expense you would expect from doing these studies via CFD alone. These methods are also useful for visualizing and gaining intuition about this complex design space, which would be difficult to accomplish using other available methods.

APPENDICES

APPENDIX A

25D Equivalent Area Distributions, Continuous Deformation Optimization Methods and Inputs, and sBOOM Atmospheric Profiles

A.1 25D Equivalent Area Distributions

The NASA 25D equivalent area distributions that were used in these studies can be found through the USU Aerolab's GitHub account [1]. The data there represents position and area in units of m and m^2 respectively.

A.2 Continuous Deformation Optimization Methods and Inputs

The cubic spline was defined using 28 nodes between 0 and 40 m which resulted in a spacing of approximately 1.482 m between each node. Only the nodes between 0 and 36 m, totalling 24, were activated and used in the optimization. The active node restriction was implemented to constrain deformations to regions of the equivalent area curve that represent Mach plane slices through the physical body of the aircraft. The additional inactive nodes between 36 and 40 m helped to force the spline back to zero in those locations. The y bounds used for each node was ± 0.075 m^2 unless the node was positioned in the first 6 m of the equivalent area distribution, in which case the lower bound for the node was set as the negative of the y value of the equivalent area distribution at that nodes location. This was done to avoid solutions that resulted in negative area values at the front of the signature where the magnitude of the deformations were large enough to cause this issue. Additional values that were used in the SciPy SLSQP method described previously are included here.

```
'ftol': 1e-05
'eps': 1.4901161193847656e-05
'maxiter': 500
```

[1] https://github.com/usuaero/rapidboom

A number of different approaches were used in generating initial guesses for the studies done using the continuous deformation method and a general description will be given here with details related to the specific studies being omitted. First, an initial guess of all zero y values could be used. Second, an initial guess using the solution from the 5 PLdB standard atmosphere study could be used. Third, a progressive approach using solutions with smaller PLdB constraints could be used. For example, a study looking to achieve a 5 PLdB reduction might start with a 1 PLdB goal and then incrementally find solutions for 2, 3, and 4 PLdB goals which would each be used as the initial guess for the following larger PLdB goal study. A combination of each off these initial guess approaches were used to find the best solution in each of the studies presented in this work.

A.3 sBOOM Atmospheric Profiles

The sBOOM presb.input files used in the flight path study presented in the current work are included here for convenience.

Boise

```
signature.data   signature_filename    0.001        padding_tolerance
1.6              mach_number           1e-06        input_tolerance
50000            altitude              2            input_format
540.026264       propagation_start     2703.6090104   altitude_stop
40000            propagation_points    1            num_azimuthal
8000             padding_points        0            azimuthal_angles
1                nonlinear             1            input_temp
1                thermoviscous         31
1                relaxation            206.0   39.12713764855347
0.01             step_size             411.2   36.65156718346559
1.9              reflection_factor     620.7   34.22730525645759
1000             resampled_points      834.7   32.005773426583914
```

```
1053.8  30.08392279825141
1507.1  24.12015846653451
1981.5  17.588884866626064
2479.6  11.430235267257785
3004.8  4.457447989465333
3559.9  -3.27671425108948
4149.0  -11.074925046479777
4778.9  -17.977689008818025
5458.2  -24.78396966126398
6198.3  -30.050781684783963
7016.8  -34.87712865926203
7929.6  -44.53048460648954
8954.7  -56.34241256737663
10137.1 -64.11470876603542
11568.3 -64.8464048010284
13414.2 -67.12313235460661
15959.1 -81.00106857038877
18119.1 -92.61113394567414
20106.4 -100.79299401631769
23033.2 -110.4194647115265
25372.4 -96.24227121845541
29740.8 -43.36585690225219
32271.1 -2.2161976227920164
34866.9 28.164703531790188
38942.0 30.81400902769176
42178.5 32.42178558227545
47696.3 25.31614525668035
4            input_wind
31
206.0   3.4235542236207603
411.2   3.4238301213905094
620.7   3.4238155443645595
834.7   3.7315612224927945
1053.8  5.541179749970773
1507.1  6.003247514097787
1981.5  7.202904307384696
2479.6  7.625012765341744
3004.8  7.623112161833766
3559.9  8.499537607076892
4149.0  9.202508649088857
4778.9  10.912924458121768
5458.2  13.685265998266225
6198.3  13.612524437106138
7016.8  13.000777342688574
7929.6  12.353618784047626
8954.7  12.630774571002028
10137.1 17.466775084453598
11568.3 24.712910226564425
13414.2 30.304509318758022
15959.1 35.2752565173359
18119.1 36.3132941171875
20106.4 37.03272793323899
23033.2 49.89912973547555
25372.4 63.027444272827154
29740.8 76.8034139288292
32271.1 65.66476857131576
```

```
34866.9 47.24647053876685
38942.0 15.818535433082095
42178.5 -5.320761013221747
47696.3 -26.7959577526207
31
206.0   -0.5668588448417591
411.2   -0.5652181939628902
620.7   -0.5677010107225063
834.7   -0.7117475261231806
1053.8  -1.7256352534536292
1507.1  -3.605248914405494
1981.5  -5.318571020091733
2479.6  -7.914450576588617
3004.8  -7.830238447391035
3559.9  -7.104442528501268
4149.0  -7.7176967254798186
4778.9  -10.346098867531746
5458.2  -15.166423986409136
6198.3  -24.168140528572955
7016.8  -36.2605912318191
7929.6  -40.51496226742742
8954.7  -30.77528647165201
10137.1 -13.331500021845786
11568.3 -9.01400335204766
13414.2 -2.364477158851886
15959.1 -1.6669749337559723
18119.1 -2.910466417991155
20106.4 0.0785160780683832
23033.2 3.5367889429092463
25372.4 9.871649611298565
29740.8 30.28196284849549
32271.1 33.18150324058533
34866.9 31.704622986731522
38942.0 12.78849626979827
42178.5 0.2951286703860698
47696.3 -12.407986447859294
1               input_humidity
31
206.0   81.20309705108652
411.2   81.20309705108652
620.7   81.20309705108652
834.7   80.57483030262766
1053.8  79.0932835475484
1507.1  82.12584286199767
1981.5  89.43304702638254
2479.6  87.98203075333035
3004.8  91.3303877882386
3559.9  95.58382386906821
4149.0  83.41850736280843
4778.9  58.77337782145915
5458.2  23.45904383260501
6198.3  10.243297261567879
7016.8  5.300494340284104
7929.6  8.388060344888904
8954.7  11.801629499849778
10137.1 13.06715493430661
```

```
11568.3 6.022753656501768
13414.2 0.40465290568312995
15959.1 2.4509414967858785
18119.1 7.458388417497158
20106.4 16.80716045883704
23033.2 46.86179127309801
25372.4 10.118007206130976
29740.8 0.1574230030449404
32271.1 0.009999999776482582
34866.9 0.0009999999310821295
38942.0 0.0009999999310821295
42178.5 0.0011999999405816197
47696.3 0.0009999999310821295
0.0          heading_angle
0.0          climb_angle
0            output_format
2            input_xdim
0            adjoint
4            objective
0.0          acceleration
0.0          turn_rate
0.0          climb_rate
0.0          3D_earth
```

Dallas

```
signature.data   signature_filename   2            input_format
1.6          mach_number              616.6010696   altitude_stop
50000        altitude                 1            num_azimuthal
540.026264   propagation_start        0            azimuthal_angles
40000        propagation_points       1            input_temp
8000         padding_points           31
1            nonlinear                207.7   32.2814190340516
1            thermoviscous            409.8   28.594404702104544
1            relaxation               615.7   26.14456482415044
0.01         step_size                828.8   37.69910889038219
1.9          reflection_factor        1053.6  46.18339056235241
1000         resampled_points         1528.1  48.48268658761359
0.001        padding_tolerance        2029.6  44.7690183641688
1e-06        input_tolerance          2558.1  38.73444423812755
```

```
3116.2  33.51776003435439
3708.9  27.85929749300302
4341.5  22.060928876167146
5019.6  14.981659403512072
5750.6  7.221037141286672
6544.4  -1.2284561949816037
7413.4  -11.608765472662853
8372.9  -24.817093500562677
9443.1  -40.823572654669704
10660.4 -58.826293134514685
12110.9 -55.03817627668087
13977.3 -72.58057146145443
16449.2 -94.1179434043676
18551.5 -96.90225334264585
20569.2 -83.68422724542901
23780.3 -66.08151602072626
26369.6 -68.92146052756218
30774.4 -65.22649739418145
33089.6 -56.698945430689676
35306.8 -52.13783399774837
38806.1 -22.553348125774505
41748.1 -7.518959108243919
46894.1 -0.7246215830553737
4             input_wind
31
207.7   0.8595668257648799
409.8   0.7129741236188156
615.7   -1.5302703491263017
828.8   -5.975304102096556
1053.6  -5.330019405711589
1528.1  2.629682771816711
2029.6  7.565358691883572
2558.1  6.996508970350458
3116.2  6.283249362585937
3708.9  5.701874251596915
4341.5  6.2463866739047536
5019.6  7.0472154125634345
5750.6  6.960480706956973
6544.4  6.828855620043566
7413.4  6.317694665087802
8372.9  6.102029357542053
9443.1  4.21934895020509
10660.4 5.725670917474362
12110.9 29.284614794416804
13977.3 23.303424559320053
16449.2 21.111926599647518
18551.5 11.035606391325372
20569.2 3.0317395508220137
23780.3 -10.832302055128675
26369.6 -14.665671645091253
30774.4 -15.917201902666282
33089.6 -9.992184988044555
35306.8 -3.9404652956996946
38806.1 -4.574930377700229
41748.1 -2.700951537449451
46894.1 8.12261842249718
```

```
31
207.7   -7.4361949082384085
409.8   -9.73039555430756
615.7   -11.06630326312084
828.8   -6.262778132200218
1053.6  0.10889263085470124
1528.1  4.993552410328673
2029.6  7.866579250983634
2558.1  8.515743668398112
3116.2  10.820587399569625
3708.9  13.825398398455068
4341.5  16.36527781487447
5019.6  18.322549807277873
5750.6  20.016649180228036
6544.4  22.56714113448904
7413.4  25.373436597713457
8372.9  28.025604448798358
9443.1  30.825151930871186
10660.4 35.995081393900286
12110.9 42.40506039053419
13977.3 43.629346966207876
16449.2 31.95351240312271
18551.5 20.254613392458346
20569.2 13.143322749855994
23780.3 3.2640633086933573
26369.6 4.412519315646932
30774.4 5.158823850174904
33089.6 -1.7325451559032174
35306.8 -7.836549396752832
38806.1 -9.342035366651533
41748.1 -12.728543149729155
46894.1 -12.589005596696087
1             input_humidity
31
207.7   82.16019506186223
409.8   87.86067836270453
615.7   94.27659635944829
828.8   98.7398348403061
1053.6  95.92615129014433
1528.1  94.96149319816132
2029.6  95.12413346826938
2558.1  96.76001120764312
3116.2  93.86434671748813
3708.9  96.88590398938751
4341.5  98.27502872111816
5019.6  98.956640136586
5750.6  99.126489273172
6544.4  99.5147164
7413.4  99.92720733658601
8372.9  100.0
9443.1  100.0
10660.4 100.0
12110.9 9.782724932908717
13977.3 4.329392106500823
16449.2 8.271415955692774
18551.5 12.534445602038772
```

```
20569.2 6.160723880177216
23780.3 0.800000011920929
26369.6 0.9032400129556659
30774.4 1.0164719842910768
33089.6 0.4067461911163628
35306.8 0.17610123729491545
38806.1 0.013913700265605566
41748.1 0.003801658007404208
46894.1 0.001299999887123704
```

```
0.0          heading_angle
0.0          climb_angle
0            output_format
2            input_xdim
0            adjoint
4            objective
0.0          acceleration
0.0          turn_rate
0.0          climb_rate
0.0          3D_earth
```

Denver

```
signature.data   signature_filename   1            num_azimuthal
1.6              mach_number          0            azimuthal_angles
50000            altitude             1            input_temp
540.0262640000001   propagation_start 31
40000            propagation_points   110.8   43.469727226935575
8000             padding_points       317.9   41.20910948882714
1                nonlinear            529.4   38.66186925594044
1                thermoviscous        745.4   36.129031363827245
1                relaxation           966.2   33.53925985388871
0.01             step_size            1423.1  28.21365148250294
1.9              reflection_factor    1902.0  22.209353254625036
1000             resampled_points     2405.2  16.361423504357447
0.001            padding_tolerance    2937.5  11.619358326772396
1e-06            input_tolerance      3504.4  8.857610707736342
2                input_format         4111.8  3.9457897745702795
5237.7626348   altitude_stop          4765.0  -1.3731716555517295
```

```
5471.1  -7.578232737979469
6237.8  -18.187117030503906
7069.8  -32.70099922048924
7981.0  -46.49399727675396
9004.6  -56.10256973707422
10188.2 -62.61397778893016
11642.3 -55.22253827197943
13533.6 -57.65270485802883
16138.6 -71.5369965625644
18376.4 -73.8142853373819
20487.6 -72.95690484903608
23714.0 -70.15395824815525
26278.3 -71.14870775770405
30683.3 -64.39302584221386
32998.4 -57.401898186204534
35209.3 -54.20496264641986
38603.1 -46.36155523726413
41370.5 -32.325751746585425
46295.1 -14.70431205528758
4            input_wind
31
110.8   -1.0315115028795316
317.9   -1.0334673699533632
529.4   -1.033105763280065
745.4   -1.0347335856696966
966.2   -1.0315679774039532
1423.1  -1.031479749425352
1902.0  -2.262459478255349
2405.2  -2.278534754470297
2937.5  -0.5728215783078575
3504.4  1.8690874677155183
4111.8  2.619848992207335
4765.0  1.064485556111691
5471.1  0.4533782893644134
6237.8  -0.47386880637932083
7069.8  -0.05076469177568503
7981.0  6.8052620131644295
9004.6  9.191929320765981
10188.2 10.159548779795214
11642.3 12.884052014067375
13533.6 14.622845292528998
16138.6 10.9016432926651
18376.4 2.9622452818900333
20487.6 -1.5195031264588579
23714.0 -6.497852781200411
26278.3 -10.444479503847049
30683.3 -15.290330104418038
32998.4 -12.72169694242478
35209.3 -7.392602523630531
38603.1 6.86393643107589
41370.5 22.89001212313262
46295.1 39.232527032470685
31
110.8   -2.7026143790160257
317.9   -2.70276020235587
529.4   -2.704085545489338
```

```
745.4   -2.7054619370909005
966.2   -2.7054400025816236
1423.1  -2.7067582815882765
1902.0  -3.3106569424991448
2405.2  -4.777724687344306
2937.5  -6.772914319351308
3504.4  -6.6575552625648875
4111.8  -5.0758624378264
4765.0  0.25942908164669437
5471.1  8.421498165549124
6237.8  16.165545870924674
7069.8  18.352957480131366
7981.0  24.86765698619657
9004.6  36.5173190904504
10188.2 36.901470262527425
11642.3 21.150026390091533
13533.6 13.697447885536649
16138.6 10.781968514555967
18376.4 1.4592807796922058
20487.6 -1.6292687199803502
23714.0 -7.341863128400721
26278.3 -11.542851061178125
30683.3 -18.818723548341666
32998.4 -19.540688272800896
35209.3 -21.31062593786803
38603.1 -23.64275854426512
41370.5 -20.312774415885304
46295.1 -13.06947048795135
```

```
1               input_humidity
31
110.8   96.03590589882934
317.9   96.03590589882934
529.4   96.03590589882934
745.4   96.03590589882934
966.2   96.03590589882934
1423.1  96.03590589882934
1902.0  98.06426116563108
2405.2  98.07640400205075
2937.5  99.25561478602174
3504.4  98.83728166891845
4111.8  99.8450382500891
4765.0  100.0
5471.1  99.98052085572023
6237.8  99.99721726786011
7069.8  99.88282595231814
7981.0  82.30975160740509
9004.6  21.553831426903052
10188.2 22.32568728487819
11642.3 1.9253256351054893
13533.6 0.5794807555304142
16138.6 2.981403058227729
18376.4 3.8806439872972103
20487.6 3.8052900094509132
23714.0 2.3531299655366515
26278.3 1.6748900408422651
30683.3 0.7281614256269072
```

32998.4 0.36220130203334794

35209.3 0.19488100397586808

38603.1 0.06615059086632069

41370.5 0.018024975193803007

46295.1 0.0024990297129377725

0.0 heading_angle

0.0 climb_angle

0 output_format

2 input_xdim

0 adjoint

4 objective

0.0 acceleration

0.0 turn_rate

0.0 climb_rate

0.0 3D_earth

Miami

signature.data signature_filename 1 input_temp

1.6 mach_number 31

50000 altitude 120.3 76.78997957336703

540.0262640000001 propagation_start 342.5 73.24060459641632

40000 propagation_points 568.9 69.70693415358379

8000 padding_points 799.8 67.19188977973526

1 nonlinear 1035.6 64.44864018913972

1 thermoviscous 1522.9 58.66909297438864

1 relaxation 2033.7 53.18572388927585

0.01 step_size 2572.4 48.68289678833146

1.9 reflection_factor 3143.0 43.83417341477432

1000 resampled_points 3749.1 38.06691125739495

0.001 padding_tolerance 4395.8 32.3212320660401

1e-06 input_tolerance 5090.3 26.543410858907396

2 input_format 5840.7 19.548185801789963

2.6902888 altitude_stop 6656.9 11.453847545776398

1 num_azimuthal 7551.6 1.6436875166929568

0 azimuthal_angles 8541.3 -10.542287874920262

```
9648.9  -25.902622767873616
10907.0 -45.285177082376805
12366.4 -69.75145926065348
14142.4 -88.27050635169417
16553.0 -96.88041669959452
18648.9 -94.88854940528304
20696.2 -77.57403047525045
23928.6 -65.55578669097896
26554.1 -56.56439871328638
31180.5 -44.12759882713803
33608.1 -37.8691751317652
35937.4 -29.47822757134037
39607.6 -6.096151583720186
42642.7 5.663393107229261
47908.0 6.650516286081416
4            input_wind
31
120.3   -6.340775397920178
342.5   -6.664166061713848
568.9   -6.798968805779333
799.8   -6.66834503913063
1035.6  -6.281541688721495
1522.9  -7.3401869867743414
2033.7  -7.132647146123802
2572.4  -4.663003465410926
3143.0  -3.4281143031832704
3749.1  -3.557035166640659
4395.8  -2.7290485955235115
5090.3  -1.520276882190998
5840.7  -1.779239969914969
6656.9  -1.4941862717315648
7551.6  0.20527650379715726
8541.3  3.197182647931924
9648.9  6.839255252261155
10907.0 12.453666442085057
12366.4 16.248155958645725
14142.4 22.900366116475524
16553.0 6.295824125208084
18648.9 0.458543306324949
20696.2 -3.6858075818095672
23928.6 -13.531729728533096
26554.1 -14.740777397648962
31180.5 -9.988224136166725
33608.1 -11.174356546448248
35937.4 -11.571691158492182
39607.6 -13.603164183858318
42642.7 -16.500188899897424
47908.0 -24.286958938209537
31
120.3   2.510482897747912
342.5   2.8991967209365854
568.9   3.373515449262377
799.8   3.9909731251654628
1035.6  4.338946839082622
1522.9  3.9371739465665563
2033.7  5.254836545861342
```

```
2572.4  6.711055539599311
3143.0  6.546464857412049
3749.1  6.6115155221148765
4395.8  7.485206942492665
5090.3  8.305415292878084
5840.7  7.263014906589889
6656.9  7.107660512471895
7551.6  8.141672512790016
8541.3  9.442979422418064
9648.9  11.307415720206663
10907.0 15.076632634719621
12366.4 20.586563442927936
14142.4 11.403859447441693
16553.0 -3.6867371848171335
18648.9 -5.25050404548645
20696.2 -2.6371741679668426
23928.6 0.5947095199864292
26554.1 -2.7753836489405157
31180.5 -2.9436354633665704
33608.1 -1.6533290701229189
35937.4 -1.4413249119220397
39607.6 -2.647133444906264
42642.7 -1.7927952305340908
47908.0 -1.4305342955555465
1            input_humidity
31
120.3   79.44740169023545
342.5   84.02336504850356
568.9   86.87425282777694
799.8   83.90641069081619
1035.6  76.23165874935867
1522.9  68.35699104128699
2033.7  79.63917102986281
2572.4  88.27764452412109
3143.0  93.51500420091446
3749.1  96.38703343642197
4395.8  99.09936907772507
5090.3  99.26093190320664
5840.7  99.32249155786653
6656.9  99.58862485110353
7551.6  99.95429406
8541.3  100.0
9648.9  100.0
10907.0 100.0
12366.4 100.0
14142.4 84.95525128589189
16553.0 12.742163389662455
18648.9 10.280551627696628
20696.2 4.9146085337605
23928.6 1.7330506211560175
26554.1 0.699999988079071
31180.5 0.1954294089121251
33608.1 0.07999999821186066
35937.4 0.03999999910593033
39607.6 0.009999999776482582
42642.7 0.0020000000949949026
```

```
47908.0 0.0013000000035390258
0.0             heading_angle
0.0             climb_angle
0               output_format
2               input_xdim
0               adjoint
4               objective
0.0             acceleration
0.0             turn_rate
0.0             climb_rate
0.0             3D_earth
```

Seattle

```
signature.data   signature_filename    34.4    34.40007965452166
1.6             mach_number            237.8   32.30039561008461
50000           altitude               445.5   29.68257522522341
540.0262640000001   propagation_start  657.4   26.559877037960213
40000           propagation_points     873.7   23.536585195221413
8000            padding_points         1320.6  17.543724165916455
1               nonlinear              1788.7  11.789707919758133
1               thermoviscous          2280.7  5.4548711074447525
1               relaxation             2799.0  -1.6277833584133603
0.01            step_size              3346.6  -9.453400556113984
1.9             reflection_factor      3927.3  -18.00052812935254
1000            resampled_points       4545.7  -27.405867027229263
0.001           padding_tolerance      5208.5  -36.40498814204007
1e-06           input_tolerance        5927.4  -43.32212440647129
2               input_format           6719.0  -49.43376128301233
173.2611604    altitude_stop           7602.3  -56.0644615069847
1               num_azimuthal          8607.8  -60.313976973396464
0               azimuthal_angles       9788.8  -62.32072546320711
1               input_temp             11224.7 -65.88561359220098
31                                     13051.8 -72.45258920818705
```

```
15580.6 -79.10597860299681
17766.9 -86.82095928716271
19789.8 -92.47806449102013
22831.9 -93.59069444557568
25262.1 -85.34206445808786
29795.1 -25.371227179443416
32353.3 -15.17225608280554
34796.5 -11.159377562343785
38489.2 -22.06230011322019
41352.5 -26.372488657531697
46288.8 -15.235983012043057
4             input_wind
31
34.4    -0.521004940557356
237.8   -0.8133301422106307
445.5   -0.15768594104840694
657.4   0.3049531123772609
873.7   1.2274766502879944
1320.6  2.3371570722562636
1788.7  4.506762369477483
2280.7  6.06628114667769
2799.0  6.992159203813081
3346.6  7.392891406076296
3927.3  7.031600118922769
4545.7  6.21441984038308
5208.5  7.486885789635984
5927.4  9.725757424569933
6719.0  11.84220478307787
7602.3  13.30687189306803
8607.8  15.829196485783347
9788.8  19.752412257634425
11224.7 25.252998257038428
13051.8 31.763076522663997
15580.6 36.59845296081612
17766.9 37.687939311743165
19789.8 37.13643615730874
22831.9 37.437850522311024
25262.1 38.17424268031861
29795.1 17.259452763217844
32353.3 10.531502235336172
34796.5 11.653336052332557
38489.2 12.265921690494137
41352.5 18.861425969698445
46288.8 25.682518550323746
31
34.4    1.0904710126728725
237.8   2.06215144628257
445.5   3.012490316171347
657.4   3.276520271691953
873.7   3.659109582983322
1320.6  3.5641245692579533
1788.7  3.2330040927236423
2280.7  3.0234112904916755
2799.0  3.332007109906035
3346.6  3.5542527204183934
3927.3  3.859689478547755
```

```
4545.7  4.394082916489954
5208.5  5.267123157176485
5927.4  5.1633893343263795
6719.0  2.6334525877065706
7602.3  -0.5955505736033908
8607.8  -3.0870292271593667
9788.8  -6.813243216974614
11224.7 -8.840464928326096
13051.8 -10.530193821214507
15580.6 -19.079797594426537
17766.9 -21.87559391274597
19789.8 -23.456173275331878
22831.9 -18.21983223056793
25262.1 -15.06165872347185
29795.1 -4.54446449703263
32353.3 -0.21520928162040925
34796.5 -2.2557008124938616
38489.2 -1.970752264117288
41352.5 -0.5211862561063406
46288.8 -3.2874868725454407
1             input_humidity
31
34.4    90.28819302042132
237.8   88.2603120831563
445.5   87.82747461636066
657.4   90.80334776498219
873.7   92.11265327112903
1320.6  92.83921739077778
1788.7  93.75986917633671
2280.7  96.2275224088466
2799.0  98.80006249458528
3346.6  99.40781374274141
3927.3  99.23206728178224
4545.7  99.86686908348192
5208.5  84.01359795781639
5927.4  41.08289012646757
6719.0  15.491383647474748
7602.3  11.313762565623477
8607.8  9.548277690893224
9788.8  5.092496216117095
11224.7 1.5480576350481359
13051.8 1.5961918922586713
15580.6 3.3949381043056013
17766.9 7.378468766262617
19789.8 11.836242248138085
22831.9 11.322101014514597
25262.1 4.463277148618468
29795.1 0.05393799992352723
32353.3 0.019999999552965164
34796.5 0.009999999776482582
38489.2 0.01480751920742156
41352.5 0.012840887902999785
46288.8 0.0029061699670040984
0.0           heading_angle
0.0           climb_angle
0             output_format
```

```
2               input_xdim
0               adjoint
4               objective
                0.0             acceleration
                0.0             turn_rate
                0.0             climb_rate
                0.0             3D_earth
```

REFERENCES

[1] Maglieri, D. J., Bobbitt, P. J., Plotkin, K. J., Shepherd, K. P., Coen, P. G., and Richwine, D. M., "Sonic Boom: Six Decades of Research," Technical Report NASA/SP-2014-622, NASA, 2014.

[2] Federal Aviation Regulations, "14 C.F.R. §91.817, Civil aircraft sonic boom," 2019.

[3] Pawlowski, J. W., Graham, D. H., Boccadoro, C. F., Coen, P. G., and Maglieri, D. J., "Origins and Overview of the Shaped Sonic Boom Demonstration Program." *AIAA Paper 2005-0005*, 2005.

[4] Anderson, J., *Modern Compressible Flow, 3rd Edition*, McGraw-Hill Education, New York, N.Y., 2017.

[5] Rallabhandi, S., *Sonic Boom Minimization through Vehicle Shape Optimization and Probalistic Acoustic Propagation*, Ph.D. thesis, Georgia Institute of Technology, Atlanta, 2005.

[6] Ordaz, I., Geiselhart, K. A., and Fenbert, J. W., "Conceptual Design of Low-Boom Aircraft with Flight Trim Requirement," *Journal of Aircraft*, Vol. 52, No. 3, 2015, pp. 932–939.

[7] Li, W. and Rallabhandi, S. K., "Inverse Design of Low-Boom Supersonic Concepts Using Reversed Equivalent-Area Targets," *Journal of Aircraft*, Vol. 51, No. 1, 2014, pp. 29–36.

[8] Chan, M. K., *Supersonic Aircraft Optimization for Minimizing Drag and Sonic Boom*, Ph.D. thesis, Stanford University, Standford, 2003.

[9] Park, M. A. and Nemec, M., "Nearfield Summary and Statistical Analysis of the Second AIAA Sonic Boom Prediction Workshop," *35th AIAA Applied Aerodynamics Conference*, 2017.

[10] NASA, "Sonic Boom Heads for a Thump," 2018-04-3 (Accessed 2020-11-10), https://www.nasa.gov/topics/aeronautics/features/sonic_boom_thump.html.

[11] Lazzara, D. S., Magee, T., Shen, H., and Mabe, J. H., "Off-Design Sonic Boom Performance for Low-Boom Aircraft," *AIAA Scitech 2019, San Diego*, 2019.

[12] Giblette, T. and Hunsaker, D. F., "Prediction of Sonic Boom Loudness Using High-Order Panel Methods for the Near-Field Solution," *AIAA Scitech 2019, San Diego*, 2019.

[13] Derbyshire, T. and Sidwell, K. W., "PAN AIR Summary Document," NASA Contractor Report, Boeing Military Airplane Company, Seattle, WA, 1982.

[14] Giblette, T., *Rapid Prediction of Low-Boom and Aerodynamic Performance of Supersonic Transport Aircraft Using Panel Methods*, Master's thesis, Utah State University, Logan, UT, 2019.

[15] Bolander, C. R. and Hunsaker, D. F., "Near-field Pressure Signature Splicing for Low-Fidelity Design Space Exploration of Supersonic Aircraft," *AIAA Scitech 2020, Orlando*, 2020.

[16] Rallabhandi, S. K., "Advanced Sonic Boom Prediction Using the Augmented Burgers Equation," *Journal of Aircraft*, Vol. 48, No. 4, 2011, pp. 1245–1253.

[17] Bolander, C. R., Hunsaker, D. F., Shen, H., and Carpenter, F. L., "Procedure for the Calculation of the Perceived Loudness of Sonic Booms," *AIAA Scitech 2019, San Diego*, 2019.

[18] Stevens, S., "Perceived level of noise by Mark VII and decibels (E)," *The Journal of the Acoustical Society of America*, Vol. 51, No. 2B, 1972, pp. 575–601.

[19] Ashley, H. and Landahl, M., *Aerodynamics of Wings and Bodies*, Dover Publications, Inc, Mineola, N.Y., 1985.

[20] Sears, W. M., "On Projectiles of Minimum Wave Drag," *Quarterly of Applied Mathematics*, Vol. 4, 1947.

[21] Haack, W., "Geschossformen kleinsten wellenwiderstandes," *Bericht der Lilienthal-Gesellschaft*, Vol. 136, No. 1, 1947, pp. 14–28.

[22] Whitham, G. B., "The Flow Pattern of a Supersonic Projectile," *Communications of Pure and Applied Mathematics*, Vol. 5, No. 3, 1952, pp. 301–347.

[23] Plotkin, K. J., "Review of Sonic boom Theory," *AIAA 12th Aeroacoustics Conference*, 1989.

[24] Carlson, H. W. and Maglieri, D. J., "Review of Sonic-Boom Generation Theory and Prediction Methods," *The Journal of the Acoustical Society of America*, Vol. 51, No. 2C, 1972, pp. 675–685.

[25] Seebass, R. A., "Sonic Boom Theory," *Journal of Aircraft*, Vol. 6, No. 3, 1969, pp. 177–184.

[26] Darden, C. M., "Minimization of Sonic-Boom Parameters In Real and Isothermal Atmospheres," Technical Report NASA TN D-7842, NASA, 1975.

[27] Seebass, R. A. and Argrow, B., "Sonic Boom Minimization Revisited," *Theoretical Fluid Mechanics Meeting*, 1998.

[28] Ueno, A., Kanamori, M., and Makino, Y., "Multi-fidelity Low-boom Design Base on Near-field Pressure Signature," *AIAA Scitech 2016, San Diego*, 2016.

[29] Weaver-Rosen, J. M., Carpenter, F. L., Cizmas, P. G. A., Malak, R. J., Abraham, T. A., Hunsaker, D. F., and Lazzara, D. S., "Computational Design Methodology of Adaptive Outer Mold Line for Low En-Route Noise of a Supersonic Aircraft," *AIAA Scitech 2021*, 2021.

[30] Leatherwood, J. D., Sullivan, B. M., Shepherd, K. P., McCurdy, D. A., and Brown, S. A., "Summary of Recent NASA Studies of Human Response to Sonic Booms," *The Journal of the Acoustical Society of America*, Vol. 111, No. 1, 2002, pp. 586–598.

[31] Wintzer, M., Ordaz, I., and Fenbert, J. W., "Under-Track CFD-Based Shape Optimization for a Low-Boom Demonstrator Concept," *AIAA Paper 2015-2260*, 2015.

[32] Ordaz, I., Wintzer, M., and Rallabhandi, S., "Full-Carpet Design of a Low-Boom Demonstrator Concept," *AIAA Paper 2015-2261*, 2015.

[33] Galvan, E. and Malak, R. J., "P3GA: An Algorithm for Technology Characterization," *Journal of Mechanical Design*, Vol. 137, Jan. 2015.

[34] Deb, K., Pratap, A., Agarwal, S., and Meyarivan, T., "A fast and elitist multiobjective genetic algorithm: NSGA-II," *IEEE Transactions on Evolutionary Computation*, Vol. 6, April 2002, pp. 182–197.

[35] Virtanen, P., Gommers, R., Oliphant, T. E., Haberland, M., Reddy, T., Cournapeau, D., Burovski, E., Peterson, P., Weckesser, W., Bright, J., van der Walt, S. J., Brett, M., Wilson, J., Millman, K. J., Mayorov, N., Nelson, A. R. J., Jones, E., Kern, R., Larson, E., Carey, C. J., Polat, İ., Feng, Y., Moore, E. W., VanderPlas, J., Laxalde, D., Perktold, J., Cimrman, R., Henriksen, I., Quintero, E. A., Harris, C. R., Archibald, A. M., Ribeiro, A. H., Pedregosa, F., van Mulbregt, P., and SciPy 1.0 Contributors, "SciPy 1.0: Fundamental Algorithms for Scientific Computing in Python," *Nature Methods*, Vol. 17, 2020, pp. 261–272.

[36] Kraft, D., "A software package for sequential quadratic programming." *Tech. Rep. DFVLR-FB 88-28*, 1988.

[37] Lazzara, D. S., Magee, T., Shen, H., Mabe, J. H., Leal, P. B., and Hartl, D. J., "A Decoupled Method for Estimating Non-Ideal Sonic Boom Performance of Low-Boom Aircraft Due to Off-Design Flight Conditions and Non-Standard Atmospheres," *AIAA Scitech 2021*, 2021.

[38] Ishikawa, H., Makino, Y., Ueno, A., and Kanamori, M., "Sonic Boom Assessment in Primary Boom Carpet of Low-Boom Supersonic Airplane (NASA C25D)," *AIAA Scitech 2019, San Diego*, 2019.

[39] Abraham, T. A., Hunsaker, D. F., Weaver-Rosen, J. M., and Malak, R. J., "Identifying Optimal Equivalent Area Changes to Reduce Sonic Boom Loudness," *AIAA Scitech 2020, Orlando*, 2020.